colloids and interfaces

MDPI

Review

Triazine 2D Nanosheets as a New Class of Nanomaterials: Crystallinity, Properties and Applications

Valery N. Zakharov, Igor K. Kudryavtsev, Sergey F. Dunaev, Kseniya A. Paseshnichenko and Leonid A. Aslanov *

Department of Chemistry, Lomonosov Moscow State University, 119991 Moscow, Russia; zakharov@struct.chem.msu.ru (V.N.Z.); ikk_49@mail.ru (I.K.K.); head@general.chem.msu.ru (S.F.D.); ervo-mveri@mail.ru (K.A.P.)

* Correspondence: aslanov.38@mail.ru

Abstract: Based on the recent (2015–2021) literature data, the authors analyze the mutual dependence of crystallinity/amorphism and specific surface area and porosity in covalent triazine frameworks (CTFs), taking into account thermodynamic and kinetic control in the synthesis of these 2D nanosheets. CTFs have now become a promising new class of high-performance porous organic materials. They can be recycled and reused easily, and thus have great potential as sustainable materials. For 2D CTFs, numerous examples are given to support the known rule that the structure and properties of any material with a given composition depend on the conditions of its synthesis. The review may be useful for elder students, postgraduate students, engineers and research fellows dealing with chemical synthesis and modern nanotechnologies based on 2D covalent triazine frameworks.

Keywords: 2D nanosheets; covalent triazine frameworks (CTFs); crystallinity; thermodynamic and kinetic control of synthesis of 2D nanosheets; surface; porosity

check for updates

Citation: Zakharov, V.N.; Kudryavtsev, I.K.; Dunaev, S.F.; Paseshnichenko, K.A.; Aslanov, L.A. Triazine 2D Nanosheets as a New Class of Nanomaterials: Crystallinity, Properties and Applications. *Colloids Interfaces* **2022**, *6*, 20. https://doi.org/10.3390/colloids6020020

Academic Editors: Alexander Kamyshny and Victor Starov

Received: 22 February 2022
Accepted: 28 March 2022
Published: 30 March 2022

Publisher's Note: MDPI stays neutral with regard to jurisdictional claims in published maps and institutional affiliations.

Copyright: © 2022 by the authors. Licensee MDPI, Basel, Switzerland. This article is an open access article distributed under the terms and conditions of the Creative Commons Attribution (CC BY) license (https://creativecommons.org/licenses/by/4.0/).

1. Introduction

The synthesis of 2D nanosheets and the study of their properties are very important pathways in modern chemistry, beginning with graphene [1]. 2D nanocrystals (nanosheets) obtained by the exfoliation of crystals [2] or chemical synthesis [3] have different properties depending on the number of layers in a nanosheet [3]: when the former exceeds 10, the properties of 2D nanosheets do not differ from the properties of bulk crystals. Therefore, the development of the methods of synthesis of 2D nanosheets with a given number of layers is required.

2D nanocrystals of monoatomic thickness (nanosheets) are easily deformed; this results in the loss of translation symmetry. It also means that monolayer 2D nanocrystals are polymers rather than crystals. Various monolayer 2D polymers—a real way to obtain monolayer planar structures—have been widely synthesized in the last ten years and named covalent organic frameworks (COF).

Beside those mentioned above, there are a lot of names for 2D polymers reflecting their specific composition, structure and properties: for example, conjugated microporous polymers (CMP), covalent polymer networks (CPN), covalent triazine frameworks (CTF), microporous organic polymers (MOP), polymers of intrinsic microporosity (PIM), porous organic networks (PON), porous polymer networks (PPN), and so on. The commonly accepted nomenclature in this new field of knowledge does not exist yet. Among the abundance of literature concerning the frameworks of nanosheets, we have considered only those published in the last seven years describing polymers composed of triazine cycles [4–155]. CTFs have become a promising new class of high-performance porous organic materials. CTFs have a series of unique characteristics, i.e., high chemical stability even in the presence of strong acids and bases. They can be recycled and reused easily and thus have great potential as sustainable materials. Due to their presence, polymers

acquire hydrophilic properties, and the larger the number of triazine cycles in a polymer, the clearer hydrophilic properties manifest themselves. Hydrophilic–hydrophobic balance is an important property for many applications of these polymers. Various CTFs are reviewed in more detail in [45,117–121].

In this review, we shall use the widely accepted abbreviation CTF. Together with this, we shall distinguish CMP from polymers without a system of conjugated bonds because of their different properties: only polymers with conjugated chemical bonds exhibit electroconductivity, whereas sorbents have any chemical bonds.

Hydrophilic–hydrophobic balance in CTFs is defined not only by triazine knots but also by linkers—CTF fragments—which join triazine knots together; carbohydrate linkers provide the hydrophobic shift of CTF properties, and the presence of heteroatoms (N or O) in the linkers promotes the enhanced hydrophilicity of polymers.

The formation and crystallization of various COFs from solution are intensively studied, but there are still a lot of "blind spots" in the kinetics of sedimentation processes. The most common problems are as follows: what type of control—thermodynamic or kinetic one—is realized during CTF synthesis? Does nucleation proceed via classical or nonclassical schemes of seed formation and growth?

The problems of thermodynamic and kinetic control in application to the synthesis of covalent organic 2D frameworks have been discussed [123–125] and postulated [126]. According to Ji et al. [124], under thermodynamic control, the distribution of reaction products is directly governed by their relative stabilities. Under kinetic control, the ratio of the reaction products is governed by the relative rates of their formation; the latter is related with the activation energies of the reactions. In turn, the reaction conditions define what type of control is realized. High reaction temperature, the presence of catalysts, and an intentionally long time of reaction and crystallization lead to the products being under conditions of thermodynamic equilibrium. On the other hand, low temperature and intentionally short reaction and crystallization time favor kinetic control. Of course, pure kinetic or thermodynamic control are ideal cases; in reality, various combinations are possible depending on parameters, and this is very important for the consideration of CTFs.

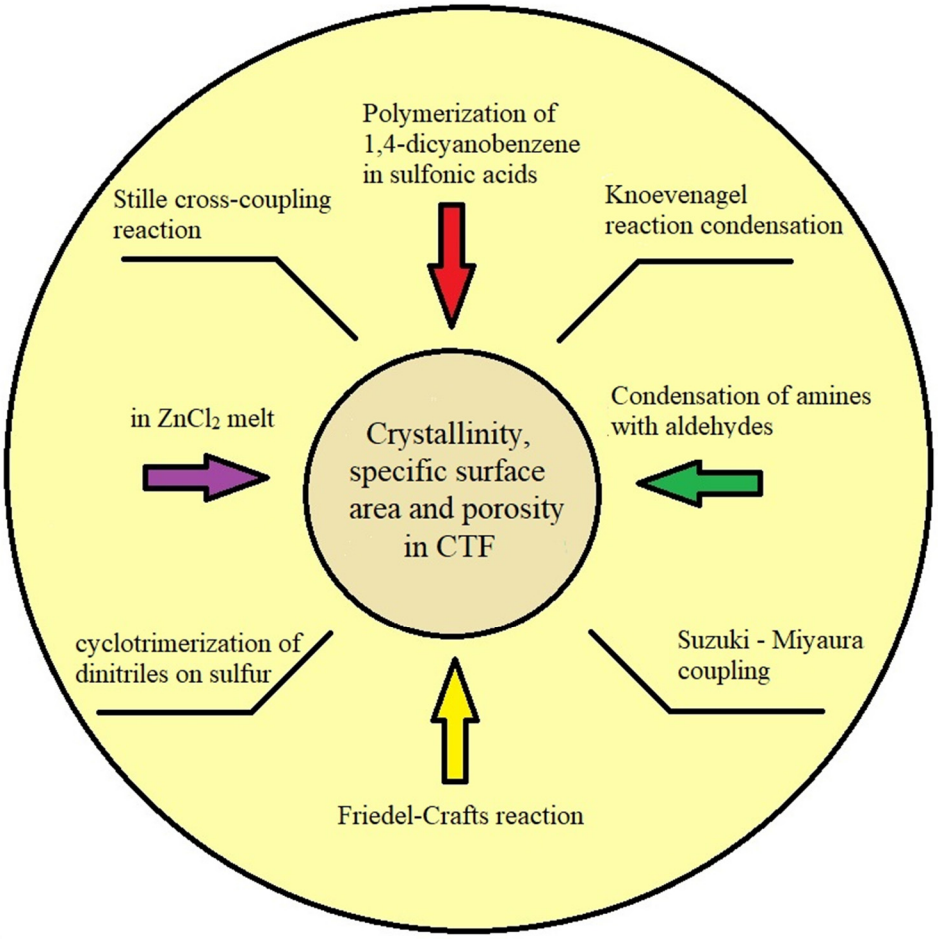
The relationships between the parameters which define the type of control governing the synthesis allow us to obtain various reaction products. Temperature, pH, reagent concentrations, microwave, mechanical and radiation effects are among these parameters.

In the course of a reaction, the reaction mixture changes towards the thermodynamic equilibrium corresponding to the absolute minimum of a system energy, but can fall into a kinetic trap [125]. Chemists use kinetic traps for a long time. For example, the quenching of a high-temperature crystalline modification of any substance in liquid nitrogen allows the study of high-temperature polymorphs at room temperature, and can even obtain amorphous metals.

The elaboration of control, thermodynamic or kinetic, of the reaction pathway allows us to control the composition and structure of materials. Besides composition and molecular structure, crystallinity and, consequently, the mechanism of formation of crystal structures from the supersaturated solution is important for materials. It is commonly accepted [130] that the seeds formed from the supersaturated solution develop according to the classical nucleation and crystal growth theory until crystals attain mesoscopic size. However, experimental data indicate that the classical theory "works" well only at a low degree of supersaturation. At significant supersaturation, the process is rather complicated [131].

So called nonclassical theory of crystallization, which explains the formation of the thermodynamically stable macroscopic phase (corresponding to the minimum of free energy) is nowadays developed. According to the new theory, the supersaturated solution transforms to colloidal solution containing amorphous particles of the crystallizing substance. The formation of crystal seeds occurs in these amorphous particles. Nonclassical theory suggests that various ordering parameters play various roles in the transformation process, and these transformations are multistep and include metastable stages.

Accounting for modern concepts, in this review we consider the effect of conditions of synthesis on crystallinity, porosity, specific surface area and properties of CTFs with various compositions (Scheme 1). Possible thermodynamic and kinetic control of the processes of the fabrication of polymeric 2D nanosheets are also analyzed.



Scheme 1. Methods of synthesis of CTFs mentioned in the text.

2. Dependence of Crystallinity, Specific Surface Area and Porosity of Ctf on Synthetic Conditions

The standard evaluations of the degree of crystallinity of CTF are rather conventional: the presence of two to four broad or weak peaks on powder diffractogram is recognized as a crystalline state of a sample, although two broad peaks can be interpreted as an amorphous state, because a similar diffraction pattern often indicates that the 3D translation symmetry is absent from the sample.

Looking forward, the main conclusion of this review is the following: a wide variety of combinations of kinetic and thermodynamic control in various steps of synthesis of 2D nanosheets result in the conclusion that the structure and properties of CTF depend on the synthetic pathway and conditions. Thus, the literature considered below is arranged based on types of chemical reactions, taking into account synthetic conditions.

2.1. Crystallinity via CTF Synthesized in $ZnCl_2$ Melt

2.1.1. Standard Conditions

Conditions for the synthesis of CTF nanosheets via the polymerization of 1,4-dicyanobenzene in $ZnCl_2$ melt are commonly accepted as the standard ones, if the reaction temperature is 400 °C, reaction time is 40–48 h, and the molar ratio $ZnCl_2$:1,4-dicyanobenzene (monomer) is about 5. Synthesis based on 1,4-dicyanobenzene yields the products commonly referred

to in the literature as CTF-1. The latter can be amorphous with a specific surface area (SSA) and a total volume of micro- and mesopores from 782.4 m^2 g^{-1} and 0.42 cm^3 g^{-1} [99] to 1270 m^2 g^{-1} and 0.63 cm^3 g^{-1} [100], respectively (herein SSA is determined by BET method). CTF-1 products can also be crystalline with SSA and a total pore volume from 537 m^2 g^{-1} and 0.45 cm^3 g^{-1} [11] to 789 m^2 g^{-1} and 0.37 cm^3 g^{-1} [102], respectively.

Crystalline state is not always detected [8,100,102–104]. Zheng et al. [8] synthesized crystalline polymer with SSA and a total pore volume of 737 m^2 g^{-1} and 0.6 cm^3 g^{-1}, respectively, whereas amorphous polymer obtained from another precursor under the same conditions had SSA and a total pore volume of 1279 m^2 g^{-1} and 1.5 cm^3 g^{-1}, respectively [8].

As a result of the adsorption of a surfactant (sodium dodecylsulfate, SDS) by CTF-1 nanolayers (monoatomic thickness,) the distance between the triazine polymer nanolayers increases from 3.4 to 4.4 Å [7], that is, SDS intercalates between CTF-1 nanolayers. The intercalation of perfluorooctanoic and perflourooctanesulfonic acids in the interlayer space of CTF-1 is reported in [100]. It should be noted that the low crystallinity of CTF-1 was accompanied by increased SSA (1270 m^2 g^{-1}) and total porosity (0.63 cm^3 g^{-1}).

Crystallization of CTFs usually results in the AA packing motif of 2D nanolayers. This fact indicates that every subsequent layer grows of the surface of the preceding one (template synthesis with self-recognition of the lower nanolayer by the growing one).

CTFs with a system of conjugated bonds in each layer (which should be planar) can be amorphous if a mixture of various dinitriles is used. The random participation of different dinitriles in a polymerization reaction results in layers without any translational symmetry even within the layer, and thus amorphous substances with high SSA and porosity are obtained, for example, 1800 m^2 g^{-1} and 1.15 cm^3 g^{-1} [32].

The considered facts allow the suggestion that the SSA and porosity of CTF increase with the increase in the linker length due to the increase in the size of the six-membered cycle and, consequently, the diameter of the channel in crystalline CTF, in a case when the synthetic pathway provides the template mechanism of crystallization.

In a CTF polymer with 2,2′-dipyridine linkers [23], SSA and porosity could seemingly coincide with these values in CTF with biphenyl linkers [8]; however, they appear to be lower: 648.59 m^2 g^{-1} and 0.40 cm^3 g^{-1} versus 1279 m^2 g^{-1} and 1.50 cm^3 g^{-1} for CTF with 2,2′-dipyridine and biphenyl linkers, respectively [23]. Unfortunately, Park et al. [23] do not mention crystallinity of the sample, and therefore it is impossible to compare crystallinities of the two samples. However, one can conclude that SSA and porosity depend not only on the linker's length. It is rather common that the values of SSA and porosity of CTF increase with complication of the monomer structure: 1401 m^2 g^{-1} and 0.844 cm^3 g^{-1} [25].

So, CTF syntheses with one precursor or a mixture of precursors under the standard conditions yield either amorphous polymers with large SSA, or relatively crystalline polymers with the lower SSA; the presence of conjugated bonds in polymers promote the formation of planar nanostructures.

2.1.2. Crystallinity via CTFs Formation of Nanolayers at Various Temperatures

CTF-1 samples obtained at 300 °C were crystallized better than most of the samples obtained under the standard conditions, their SSA being rather low—about 20 m^2 g^{-1}. The sample obtained under the similar conditions at 400 °C had an SSA of 610 m^2 g^{-1}. Porosity was not reported [10].

CTF-1 obtained at 600 °C(10 h) had a SSA of 1654 m^2 g^{-1} and a total pore volume of 1.06 cm^3 g^{-1} [9]. At elevated temperature (above 600 °C), CTF begins to carbonize, and SSA and total pore volume increase simultaneously.

For amorphous CTF based on phthalazinone, these properties are almost independent of the phthalazinone:$ZnCl_2$ ratio, but temperature increase from 400 to 600 °C results in a significant increase in SSA and total pore volume [29].

SSA of CTF with carbazole linkers increases with the increase in $ZnCl_2$ fraction, polymerization time and temperature [26].

In a series of polymers produced by Fu et al. [26], there were aceto-, acetohydrazide and ethylaceto ester groups as substituents at the N atom of carbazole being the constituent of a linker. It was shown that SSA and porosity of the product depended not only on the functional group, but also on conditions of its incorporation into a linker: before polymerization or after it.

CTF based on fumaronitrile (FUM) and 1,4-dicyanonaphthalene (DCN) are amorphous according to the X-ray data [20]. With temperature increase from 350 to 500 °C, SSA and total pore volume of CTF-FUM increase, whereas for CTF-DCN these properties are almost independent of temperature.

Tao et al. [28] state that SSA and the porosity of CTF decrease with an increase in $ZnCl_2$ content in the reaction mixture. Similar results were obtained using the following precursors: pyrimidine-2,5-dicarbonitrile, 2,6-dimethylpyridine-3,5-dicarbonitrile, 5,5′-dicyano-2,2′-dipyridine and 1,4-dicyanobenzene [31]. It also appears that gas absorption (e.g., CO_2) depends on pore volume, not SSA, and the authors suppose that nitrogen concentration in 2D nanolayers is of secondary importance.

Amorphous preparations were obtained by Artzet et al. [17] from 1,3-dicyanobenzene, 2,6-dicyanopyridine, 1,4-dicyanobenzene, 4,4′-dicyanobiphenyl at 600 °C. All the samples had increased SSA and porosity values.

Wu et al. [51] obtained amorphous CTF via the special temperature protocol by the polymerization of dinitriles containing phenylene, naphthalene or perylene fragments in the central part of a linker in a $ZnCl_2$ melt. Temperature of the synthesis did not exceed 600 °C. Such polymers have medium SSA values (1053 m^2 g^{-1}) and abundant ultramicropores, about 5.4–6.8 Å in size.

2.1.3. Crystallinity via the Fabrication of Nanolayers at High Temperature

Hao et al. [12] reported the fabrication of several instances of CTF-1 under the same conditions with variable temperatures. The degree of crystallinity of the sample obtained under the standard conditions was rather low. Syntheses at 550 and 700 °C yielded amorphous materials with a SSA of 1212 and 2482 m^2 g^{-1}, respectively [12].

Amorphous CTF was synthesized from fumaronitrile in $ZnCl_2$ melt for 20 h at 500 °C, and its SSA was not large (485 m^2 g^{-1}), annealing at 700 °C allowed to reach a SSA of 1293 m^2 g^{-1} of a partially carbonized sample [19].

When tetracyanoquinodimethane (TCNQ) was used for CTF synthesis in the $ZnCl_2$ melt, amorphous samples were obtained: the higher the temperature of synthesis, the larger was their SSA [24].

Polymerization of tetrafluoroterephthalonitrile at 400 °C resulted in the product amorphous by X-ray data, which had a medium SSA value of 817 m^2 g^{-1}. SSA increased with temperature increase: 1131, 2040 and 2162 m^2 g^{-1} at 550, 700 and 900 °C, respectively [21].

2.2. CTFs with a System of Conjugated Bonds

2.2.1. Crystallinity via the Synthesis of CTFs in $ZnCl_2$

CTF stacks are often obtained amorphous with separate islands of relatively ordered crystallites with the AA packing motif of polymeric layers; the latter give diffraction patterns allowing the definition of the unit cell dimensions.

There is a way of synthesis of CTF crystals in which the layers alternate as in bilayer hexagonal AB packing with the unit cell dimensions a = 14.52 Å, c = 6.27 Å [105]. These crystals have sizes of about a millimeter, clear facets, and can be exfoliated ultrasonically in liquid media or mechanically using a glue band. In the first case, nanosheets with the lateral dimensions of several μm and 2–3 nm thick are formed in dispersion, and in the second case the linear dimensions of nanosheets exceed 10 μm with an average thickness of 4 nm (a package of 12 2D nanosheets). Crystals are yellow; it should be noted that the synthesis of the $ZnCl_2$ melt at 400 °C and higher yields a black substance—evidence for carbonization in the course of synthesis. Such crystals are obtained from 1,4-dicyanobenzene in trifluoromethanesulfonic acid. Their SSA is negligible, 142 m^2 g^{-1}, and the width distribution

of pores is rather narrow, 0.6 nm, which is typical of crystals. That is, pore width closely coincides with the diameter of the six-membered cycle of a 2D nanolayer.

Zhu et al. [36] firstly polymerized aromatic nitriles at 400 °C with a formation of CTF, and then polymer was carbonyzed in argon at 900 °C. A melt of anhydrous $FeCl_3$ mixed with S was suggested as a solvent for CTF synthesis. Authors suppose that such solvent causes the formation of Fe-N_x sites (required for use of the reaction product) and polymer doping with S during pyrolysis. Depending on the precursor used, SSA values of these CTFs vary from 739 to 2710 142 m^2 g^{-1}. Authors [36] conclude that SSA and porosity depend on the structure of linkers effecting the structure of polymers.

It is not surprising that crystallinity, SSA and porosity depend on the pathway of synthesis. The synthesis of CTF 2D nanolayers is possible not only via the trimerization of nitriles yielding triazine six-membered cycles, but also via the synthesis of linkers yielding triazine five-membered cycles. For example, Song et al. [90] synthesized 1,2,3-triazole five-membered cycles as linkers. The brown sample (2D polymer molecules had only conjugated bonds) was amorphous by X-ray data. The calculated and experimentally obtained compositions did not coincide well, which is often the case for CTFs. The microporous polymer had an SSA of 431 m^2 g^{-1} and a wide pore size distribution with a maximum at 1.2 nm.

Je et al. [98] obtained black nanolayers from tetrafluorophthalonitrile in sulfur melt, CTFs were relatively crystalline, and their X-ray patterns did not coincide with those for the initial tetrafluorophthalonitrile and sulfur. Talapeneni et al. [97] used an analogous approach, obtaining CTF via the cyclotrimerization of 1,4-dicyanobenzene in sulfur melt. It appeared that sulfur occupied all the pores in stacks of CTF 2D nanolayers.

2.2.2. Crystallinity via Polymerization of 1,4-Dicyanobenzene in Sulfonic Acids

The polymerization of 1,4-dicyanobenzene in trifluoromethanesulfonic acid yields CTFs with low SSA values independent of their degree of crystallinity. The origin of this is in low reaction temperature, when kinetic control of reaction is most probable. Synthesis at room temperature [37] yields a substance with a low degree of crystallinity and small SSA (19 m^2 g^{-1}). Amorphous CTF was obtained by the heating of 1,4-dicyanobenzene to 100 °C for 20 min [38]. The polymer had very low SSA of 5 m^2 g^{-1} at 29.5 nm pore size and a total pore volume 0.03 cm^3 g^{-1}. The polymerization of 1,4-dicyanobenzene at the interface of two immiscible liquids at 100 °C resulted in the formation of a badly crystallized polymer, which was confirmed by X-ray diffraction [39]. Nonetheless, electron microscopy revealed a separate area with the distinct electron diffraction indicating that polymer layers were arranged in hexagonal crystal packing. Specific surface area was not large (11 m^2 g^{-1}). Layer morphology of CTF can clearly be seen in the SEM image (Figure 1).

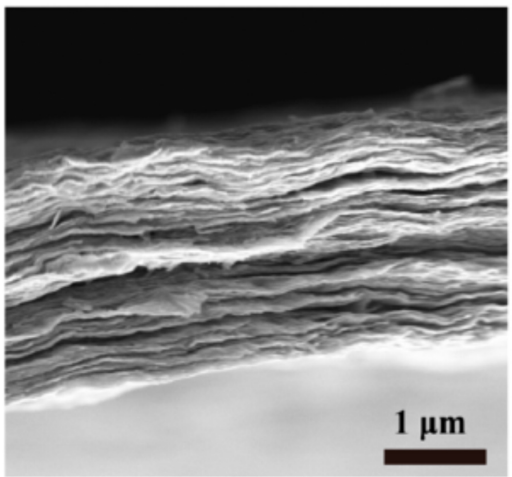


Figure 1. Scanning electron microscopy image: layer morphology of CTF [39]. Reprinted with permission from JACS, 2017, 139, 11666. Copyright 2022 American Chemical Society.

Li et al. [106] synthesized a polymer with a very poor crystallinity on the borderline, with amorphousness and its SSA being 19 m^2 g^{-1}.

A polymer obtained from 1,4-dicyanobenzene in a melt of p-toluenesulfonic acid monohydrate possessed a system of conjugated bonds [93]. The hexagonal unit cell parameters were defined as a = 12.580 Å, c = 3.418 Å; SSA was not large (535 m^2 g^{-1}).

2.2.3. Other Dinitriles

In the liquid trifluoromethanesulfonic acid, amorphous CTFs with the moderate value of SSA were obtained [40]. For example, Wang et al. [41] obtained a CTF which appeared to be a typically amorphous polymer, according to the X-ray diffraction data, in spite of the presence of a conjugated bonds system. Its SSA was 784 m^2 g^{-1}. Amorphous polymers were synthesized at 0 °C [44] and at room temperature [45], their SSA being from 625 to 896 m^2 g^{-1}, and a total pore volume from 0.32 to 0.49 cm^3 g^{-1}. A polymer obtained by Karmakar et al. [46] in the presence of TfOH, did not have a system of conjugated bonds, its SSA appeared to be 358 m^2 g^{-1} and it had a total pore volume of 0.22 cm^3 g^{-1}.

Huang et al. [42,43] synthesized CTF under conditions different from those mentioned above: polymerization proceeded in the solid state in trifluoromethanesulfonic acid vapor at 100 °C. The SSA of the three polymers synthesized in this way was negligible and did not exceed 78 m^2 g^{-1}.

So, synthesis of polymers under mild conditions yields mainly amorphous substances or structures with low crystallinity and SSA in the range from several units to 900 m^2 g^{-1}.

2.3. Crystallinity via Condensation of Amines with Aldehydes

2.3.1. Frameworks with Conjugated Bonds

The condensation of 2,4,6-*tris*-(4-aminophenyl)-1,3,5-triazine with aldehydes allows us to obtain CTFs with moderate crystallinity, limited SSA values and low porosity [48,49,52–54,60,61], but sometimes the obtained amorphous preparations have a negligible SSA, such as those of crystalline analogs [50].

El-Mahdy et al. [63] found that 2,5-diaminodihydroquinone dihydrochloride with 2,4,6-*tris*-(4-formylphenyl)-1,3,5-triazine form nanoribbons 40–50 nm in width, which form nanotubes at the longer time of synthesis. According to the powder X-ray diffraction data, unit cell parameters of hexagonal cells appeared to be as follows: a = b = 35.6565 Å, c = 3.4790 Å. The layers of polymer molecules obeyed the AA order of interposition. The SSA of crystalline polymer was rather high (1855 m^2 g^{-1}).

Yu et al. [64] showed that synthesis of CTFs via the condensation of aromatic amides of carboxylic acids in the presence of P_2O_5 resulted in the formation of s-triazine cycles. The polymer obtained at 400 °C had higher crystallinity, was more thermostable, and was likely to have higher molecular mass than that obtained at 350 °C. As shown by powder X-ray diffraction, nanosheets were packed in crystal according to the AA motif. SSA appeared to be 2034.1 m^2 g^{-1}, and there was a total pore volume 1.04 cm^3 g^{-1}. This is one more example of the effect of synthetic conditions on crystallinity and SSA. The last two examples [63,64] indicate that the crystallinity of a polymer is not always related to low SSA and porosity. Vice versa, amorphous CTFs can have very low SSA, e.g., 47.98 m^2 g^{-1} in [59]. Unfortunately, the crystallinity of CTF is not always reported, and it is impossible to establish correlation between crystallinity and SSA [22,58,70].

The synthesis of a polymer in a medium simultaneously playing the role of a template can result in very high SSA. The interaction of 3,3′-dimethylbenzidine with triformylfluoroglucinol in amino-*n*-toluenesulfonic acid (PTSA·H_2O)—the latter acted as a solvent and template [57]—yielded a substance with a SSA of 10–29 m^2 g^{-1}. However, after the removal of PTSA·H_2O with hot water, the SSA of this CTF appeared to be tremendous (2583–2933 m^2 g^{-1}).

Such results are unattainable even at CTF carbonization. Polymers with conjugated bonds were obtained by the mixing of 2,4,6-*tris*-(4-aminophenyl)-1,3,5-triazine, terephthalaldehyde and trifluoromethanesulfonic acid [62], which annealed at a temperature from

650 to 950 °C in argon. SSA increased with temperature increase: from 373 m^2 g^{-1} at 650 °C to 950 m^2 g^{-1} at 950 °C. The nitrogen content decreased simultaneously: from 7.26 to 1.51% at 650 and 950 °C, respectively. Crystallinity of the preparations was not reported.

It is not a simple task to obtain CTFs in a crystalline state. Polyimides with conjugated bonds obtained from the mixtures of melamine and dianhydride appeared to be amorphous [67].

2.3.2. Frameworks without Conjugated Bonds

If it is required to obtain CTFs with the largest values of SSA and porosity (with largest), one should preferably reject crystallinity and a system of conjugated bonds. A covalent organic framework based on triazine was synthesized under solvothermal conditions [70]. The SSA of this polymer was 882 m^2 g^{-1}, which is not low for crystalline CTF.

Crystalline COFs were synthesized [71] starting from 2,4,6-*tris*-aryloxy-1,3,5-triazine compounds. The SSA of two samples were rather high—1589 and 1441 m^2 g^{-1}. The total pore volumes were 0.92 and 1.25 cm^3 g^{-1}.

Heating of a mixture of 2,4,6-*tris*-(4-aminophenyl)-1,3,5-triazine and *tris*-(4-formylphenyl)amine yielded crystalline polymer [69] with an SSA of 2938 m^2 g^{-1}, pore sizes of 1.5 and 1.7 nm, and a total pore volume of 1.32 cm^3 g^{-1}. Such a combination of crystallinity and large SSA and porosity values is possible due to the corrugation of layers because of the presence of the triphenylamine groups. This results in a "loose" polymer and an increase in the interlayer distance between 2D nanolayers to c = 3.94 Å, whereas the usual interlayer distance is 3.3–3.6 Å. "Loose" polymers have large SSA and porosity.

However, frameworks with a large SSA are not always obtained. The covalent imine framework synthesized from melamine and 1,4-piperazinedicarboxaldehyde has a moderate SSA value of 722 m^2 g^{-1}. Crystallinity or amorphicity of the polymer is not reported. It should be noted that in spite of the absence of conjugated bonds, all the aforementioned CTFs considered in this section are crystalline.

2.4. Crystallinity via Other Methods of CTF Synthesis

CIF was obtained from 1,4-dicyanobenzene in molten *p*-toluenesulfonic acid monohydrate. A change in the solvent (in comparison with $ZnCl_2$) resulted in the surprising parameters of a hexagonal unit cell: a = 12.580 Å, c = 3.418 Å. The SSA of the sample additionally carbonized at 500 °C was 535 m^2 g^{-1} [93].

The Knoevenagel condensation reaction yields a 2D nanosheet [89] with a system of conjugated bonds containing only carbon atoms. Such a polymer is not vulnerable to hydrolysis. SEM allows the detection of nanosheets with the lateral dimensions of the tens of microns. High-resolution TEM detected pores about 2 nm in diameter, which was proved by the X-ray structural analysis. Powder X-ray diffraction revealed the AA order of the superposition of layers in a crystal. The SSA of the crystalline polymer was not high—232 m^2 g^{-1}—with a pore diameter of 12 and 22 Å. The latter value with the 10% standard uncertainty coincided with the result obtained by high-resolution TEM, whereas the former value (12 Å) corresponded with the superposition of layers according to AB order. This fact indicates irregularities in the superposition of layers (layer alternation) in AA packing. The electrochemically measured band gap of crystalline polymer was 2.36 eV, which allowed use of this polymer as a photocatalyst.

The synthesis of CTF described by Yadav et al. [95] is rather noticeable. The sample obtained seemed to be a polymer with the best crystallinity, according to the powder X-ray diffraction data. The average size of crystalline domain appeared to be 12 nm, as calculated from the Scherrer line broadening, and this is in good accordance with dimensions obtained by AFM. It was also found that most pores were 3.9 Å in diameter; SSA and porosity were not determined. The polymer did not possess the conjugated bonds system, and Yadav et al. [95] supposed that its crystallinity was caused by the structure of linkers containing perylene fragments. However, earlier, we considered a polymer with the similar linkers [59]: it was amorphous and had a small SSA value. Again, it should be

stated that the structure and properties of CTF depend on the pathways and conditions of synthesis.

In polymers with the bridging imino group [94], there are two neighboring single bonds in the polymeric chain; consequently, there is no conjugated bond system threading each CTF molecule and promoting the planarity of the polymeric nanosheet. A molecule most probably should be nonplanar due to the numerous molecular conformations; however, the crystallinity of both CTFs is satisfactory judging from their X-ray patterns, but SSA is rather low (40 and 20 m^2 g^{-1}). This is not surprising: high crystallinity is often accompanied by small SSA values. Significant crystallinity of these samples can be rationalized by the growth of each subsequent polymer layer on the preceding one as a template, repeating all the specific, occasionally formed curves of the preceding molecule (template synthesis).

Polymers with small SSA values [85,86,96] can be presented as examples of amorphous CTFs with the bridging imino groups. They do not have a system of conjugated bonds. However, a polymer with the bridging imino groups [84] and a SSA of 840 m^2 g^{-1} was obtained. The moderate value of specific surface area was possibly caused by microwave heating in the absence of a conjugated bond system. There were no data on the crystallinity/amorphicity of this sample.

Polymers obtained by the Suzuki–Miyaura reaction [87] did not have a system of conjugated bonds, and no data on its crystallinity/amorphicity were given. Polymer nanosheets were rolled into tubes about 25 μm in length, with an outer diameter of 135 nm and wall thickness of 60 nm; SSA was 409 m^2 g^{-1}.

The Friedel–Crafts reaction is often used for the preparation of nanosheets. As shown in [73,74,76,78–80,82], amorphous materials with the advanced surface are mainly formed in this reaction.

2.5. Crystallinity of CTFs as a Measure of Thermodynamic/Kinetic Control

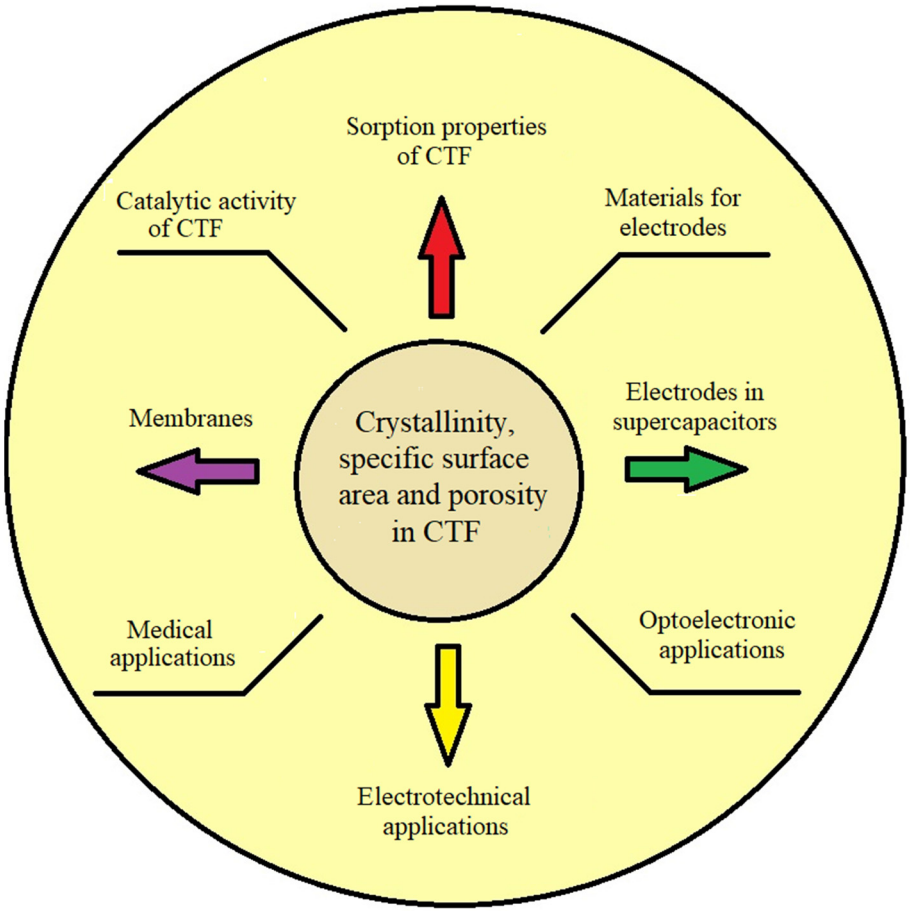
Let us choose the degree of crystallinity of a polymer as a measure of input of thermodynamic control in a polymerization reaction (together with this, let us assume that the resulting product can be a mixture of substances obtained under thermodynamic as well as kinetic control). Amorphous products will be considered as obtained under kinetic control. Such criterion of the governing type of control seems to be useful, because only crystalline substances have a thermodynamic equilibrium, whereas amorphous phases are always nonequilibrium and consequently, can be captured only by kinetic traps.

Judging by crystallinity/amorphicity, the interaction of aldehydes with amines under thermodynamic control results in predominantly porous products (accounting that other reaction conditions are similar), of which molecules possess conjugated bonds [49,53]. However, nonporous amorphous products can be also obtained [50,67]. The enhanced porosity of CTF is attained in cases when a system of conjugated bonds in a polymeric nanosheet is intensively refused, because a six-membered cycle can remain unclosed because of a violation of a system of conjugated bonds.

Unfortunately, the number of CTF syntheses performed in one and the same solvent, with one and the same catalyst, at the same reagent concentration, is insufficient for clarification of the type of control: thermodynamic or kinetic. We suppose that crystallinity is the most reliable evidence for the thermodynamic control of a reaction, because only crystalline substances can be thermodynamically stable.

3. CTF Applications

There are numerous applications of CTFs (Scheme 2) [119,152].



Scheme 2. CTF applications.

3.1. Sorption Properties of Triazine Polymers

A series of bifunctional conjugated fluorescent microporous CTFs which possess an excellent adsorption capacity of I_2 both in vapor and in solution was successfully synthesized [80,142,145]. Adsorption capacities of I_2 4.92, 4.72 and 4.49 g g^{-1} for the tested polymers are the highest known values for all COFs, up to the beginning of 2022. The authors suppose that this property is caused by high porosity, efficient sorption sites, structure and charge transfer interactions. Along with this, one of these polymers demonstrated very high sensibility in I_2 detection. These results allow the suggestion that such a polymer can be a perspective absorbent for radioactive I_2 and a sensible fluorescent I_2 tester, from the viewpoint of ecology and safety.

He et al. [108] confirmed these promising results and showed that 1 g of polymer absorbs 4.31 g I_2, which is equivalent to 96% theoretical capacity. This fact means that there are channels in the structure of polymer: iodine can reach all the adsorption centers via these channels; I_2 also has significant affinity to the conjugated π bonds—it forms charge transfer complexes with π bonds. Even with a rather low SSA of 50.5 m^2 g^{-1}, a polymer obtained from melamine and hexachlorocyclotriphosphazene [86] and containing imino groups between the triazine and triphosphazene cycles, absorbed 262 mass % I_2.

Zhao et al. [79] showed that CTFs can be used as solid-phase-extracting substance for chromatography. The polymer was successfully tested for the quantitative determination of tetracycline in meat, milk and eggs. Tetracycline (antibiotic) is often used for the medical treatment of farm animals in agriculture, and consequently it is necessary to control its content in animal products eaten by people.

One of the CTFs [76] absorbed antibiotic 5-nitroimidazole for its quantitative determination in the waste waters of the meat industry, fish farms and hospitals.

Wang et al. [144] synthesized a new CTF which demonstrated its efficiency in the solid-phase extraction of antibiotics (those of sulphonyl and tetracycline groups).

In analytical chemistry, CTFs have been used for sorption, and the extraction of eight phenols (including phenol itself, 2-chlorophenol, 2-nitrophenol, 4-nitrophenol, 2,4-dimethylphenol, p-chloro-m-cresol, 2,4-dichlorophenol and 2,4,6-trichlorophenol) from various water probes with subsequent high-performance liquid chromatography. The above-mentioned CTFs demonstrated a better extraction efficiency of the target phenol compounds compared with the commercial sorbents: a good relative extraction with a detection level in the range of 2–50 μg liter^{-1} was obtained.

Yang et al. [136] found that when CTFs are modified with thio groups, these polymers can be used for the efficient extraction of Hg^{2+} cations from aqueous solutions. The absorption capacity for Hg^{2+} attains 840 mg g^{-1}.

As shown in [138,139,146], imine-based CTFs possess good absorption properties and can be used for the extraction of dyes and chlorophenols from various industrial waste waters.

The sorption of surfactants (sodium alkylpolyglycolate and dodecylsulfate) from aqueous solutions (c = 8.0 mmol/liter) by CTF-1 polymer was reported in [7]; this exceeded the gravimetric absorption capacity of soot by more than 20 times. Authors explain such a high absorption by the exfoliation of CTF nanosheets.

Numerous studies describe gas sorption; this is natural for substances with such developed porosity as that of a CTF. As mentioned by Puthiaraj et al. [73], when one wants to obtain highly porous material for gas sorption, CTFs with 3D instead of 2D molecular structures should be synthesized. Sometimes synthesis is intentionally performed so that the structure of a polymer molecule appears to be irregular.

However, there is a drastic disproportion in the number of gas absorption studies: a lot of them are dedicated to carbon dioxide [5,9,34,35,40,49,60,64,66,85,94,140,141,146,148], and the results are rather contradictory. Shao et al. [82] state that substances with the maximal nitrogen content, not the largest SSA, are the best sorbents. Chaudhary et al. [84] also report that the increase in the nitrogen content in a polymer allows the efficient fixation of large amounts of CO_2. Zhu et al. [27] even developed a strategy for the synthesis of a new family of conjugated triazine frameworks for efficient CO_2 fixation. The specific materials thus obtained demonstrate extremely high capacity for CO_2 absorption—up to 4.8 mmol/g at 297 K and p = 1 Bar. However, Jiao et al. [31] suppose that a total volume of absorbed CO_2 depends on a total micropore volume, rather than SSA, whereas the nitrogen content in a polymer is a factor of secondary importance negligibly enhancing CO_2 sorption. The fixation of CO_2 from wet flue gases was specially studied [96].

Amorphous microporous polymers demonstrate higher CO_2 absorption, whereas CH_4 is absorbed to a lesser extent, and N_2 is absorbed only negligibly [11,20,28,39,50,72,74,93,109]. A polymer with outstanding capacity for acetylene sorption was obtained by the trimerization of nitrile in a $ZnCl_2$ melt [25]: its adsorption capacity was 104 cm^3/g at 273 K or 74 cm^3/g at 298 K. The factor of acetylene/ethylene separation was 246. This result is very important for the industrial production of polyethylene.

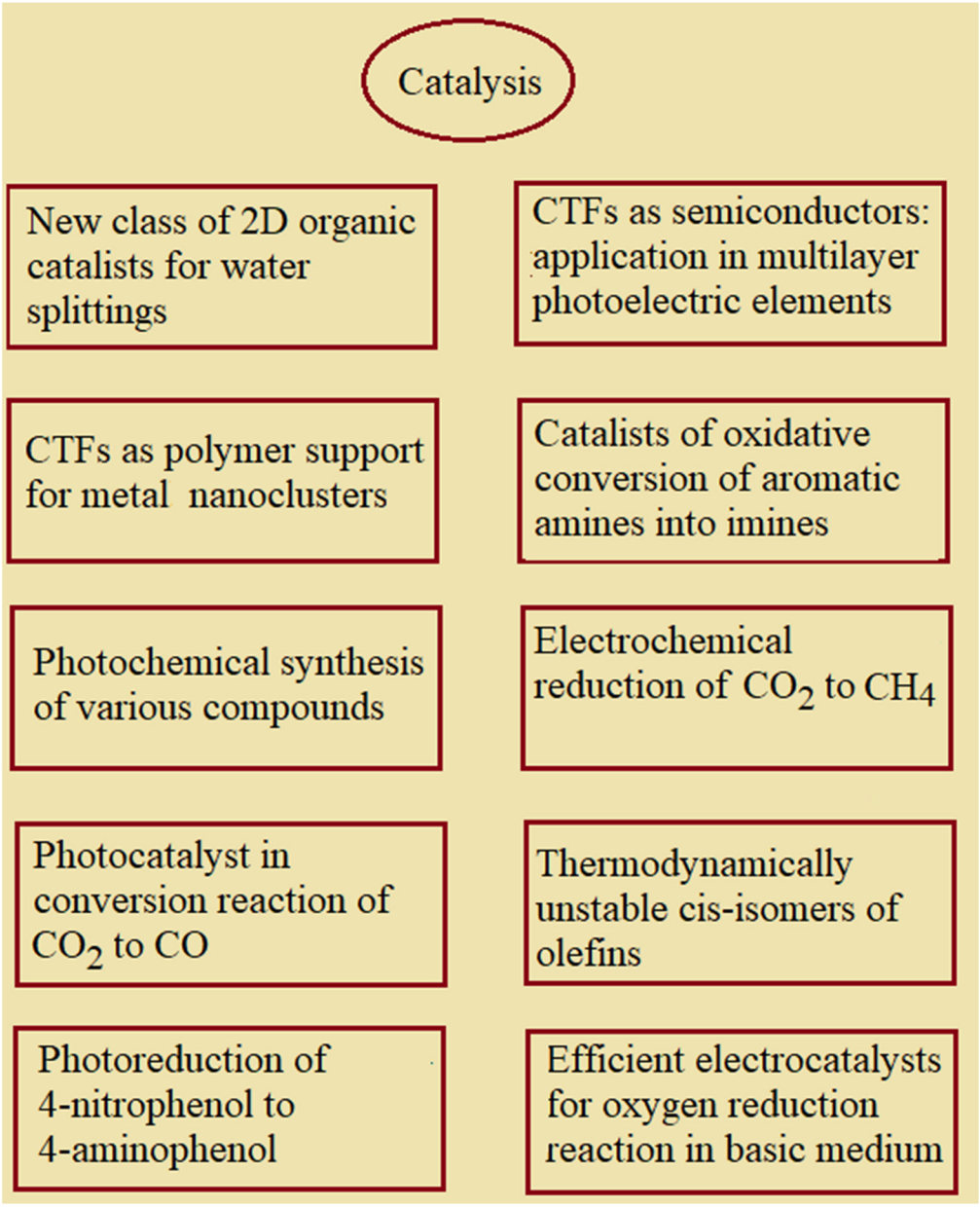
The adsorption of C_2H_2, C_2H_4 and CO_2 on CTF preparations obtained in $ZnCl_2$ melt demonstrated dependence on the arrangement of sorbent but not on its SSA [33]. The selectivity of adsorption by these polymers was within the limits of 14.5–24.5 for the C_2H_2/CH_4 gas mixture and 9.4–14.8 for the C_2H_4/CH_4 mixture.

Adsorption of hydrogen by triazine frameworks was studied in [29,31,51,71,83]. Crystalline CTF with high SSA (2034.1 m^2/g) showed high adsorption capacity for H_2 (1.75 mass % at 77 K) [64].

It is noted that CTFs can be used as efficient and sensible chemical agents for the detection of various nitroaromatic substances [44,45]. It is reported that sensibility attains 10^{-8} M for 2,4,6-trinitrophenol [53].

3.2. Catalysis

CTFs are used for different kinds of catalysis (Scheme 3). Most covalent triazine frameworks, to some extent, possess semiconductor properties. For example, crystalline CTF obtained from 2,4,6-*tris*-(4-formylphenyl)-1,3,5-triazine and 2-phenylacetonitrile [89] has a band gap width electrochemically measured to be 2.36 eV; this allows us to use this polymer as a photocatalyst. Due to the AA type of folding in crystal fragments, these CTFs possess microporosity, the band gap width decreases, and photocatalytic activity increases, including the enhanced generation of singlet oxygen.



Scheme 3. Application of CTFs in different kinds of catalysis.

The main research attention was focused on the photolysis of water to hydrogen and oxygen by the action of sunlight [10,38,112,135,137,143,147]. Studying electron band structures, energetic levels of conduction and valence bands, and optical absorption spectra, CTFs were defined as a new class of 2D organic catalyst for water splitting activated by visible light [110]. It is very important to prevent the recombination of electrons and holes in these materials, with possible microscopic origins of change in the photocatalytic activity

of polymer observed in experiments with an increase in the lateral dimensions of CTF polymeric nanosheet or with a change in the chemical composition of the polymer, as noted by Guiglion et al. [111].

Photocatalytic properties of CTFs can be enhanced by Pt nanoclusters on polymer surface. Fang et al. [37] report that Pt nanoparticles disperse well in CTF. The latter demonstrate an excellent photocatalytic activity and stable H_2 release in the presence of Pt on irradiation with visible light (420 nm). Although such studies are numerous, they consider very specific hybrid materials, and therefore we shall not discuss any more articles here.

Photochemical syntheses of various compounds are also described: for example, three CTFs with band gap widths from 2.48 to 2.30 eV [42] that is, all three were semiconductors. In the presence of such photocatalysts, the reaction of diphenylphosphine oxide with diphenylacetylene attained a 93% conversion after 24 h at illumination with white light. In the absence of a catalyst or illumination, the reaction did not proceed.

A polymer was obtained, and a system of light accumulation was constructed based on a covalently bound nanocapsule 180 nm in diameter with an envelope of 2D polymer plates [55]. In fact, a simple method for assembling donors and acceptors with the controlled donor/acceptor ratio was suggested. This new strategy for the organization of various systems of light accumulation based on the nanostructures of organic polymers can be used for the fabrication of various systems of artificial photosynthesis.

Yang et al. [87] used CTF as a photocatalyst in a conversion reaction of CO_2 to CO. The reduction of CO_2 using visible light is a traditional method for the production of valuable chemicals.

Promising photocatalytic activity of polytriazine frameworks was demonstrated in the reaction of the photoreduction of 4-nitrophenol into 4-aminophenol on irradiation by visible light [43].

CTFs demonstrate [91] a remarkable resistance to solvents and good *n*-semiconductor properties; this allows their application in multilayer organic photoelectric elements in order to increase the efficiency of solar energy transformation.

By themselves, CTFs are catalysts of oxidative (at the cost of air oxygen) conversion of aromatic amines into imines (aliphatic amines in such reactions give a yield not more than 27%). For example, CTF provided the 94% conversion of benzylamine for 10 h at 120 °C with 91% selectivity [8].

A catalyst allowing synthesis of the thermodynamically unstable *cis*-isomers of olefins was obtained by the condensation of melamine and 1,3,5-triformylfluoroglucinol [61]. The amorphous form of polymer is catalytically inactive, whereas the crystalline polymer (accounting its rather relative crystallinity) provides a 90% yield of *cis*-stilbene after an 18 h reaction with the retention of catalytic activity after four cycles.

Karmakar et al. [46] describe a CTF composed of triazine blocks with a deficit of electrons in the central knot and electron-rich aromatic linkers. Bimodal functionality of CTF was attained using benefits of the double nature of the surface of pores. A deficit of electrons in the central knot was used to solve a very important problem of the chemical industry: the separation of benzene and its saturated analog—cyclohexane. Together with this, due to the presence of electron-rich aromatic rings with the basic Lewis sites, 2,4,6-trinitrophenol, a nitro aromatic compound with high explosive potential, was detected in the aqueous phase.

Fluoro-containing CTFs [21] demonstrated catalytic activity in the electrochemical reduction of CO_2 to CH_4: the rate of methane evolution attained 7.75 mol/h m^2 at 1.2 V. If the catalyst was calcinated at 700 and 900 °C for 2h before washing and drying, fluoro-free powders unable to convert CO_2 into CH_4, in spite of the higher SSA and higher adsorption capacity of CO_2, were obtained.

CTF-1 synthesized by the ionothermal method [99] is an electrocatalyst with excellent electrocatalytic activity for the oxygen reduction reaction (ORR) in basic medium owing to

a high atomic percent of heterocyclic nitrogen, which is the most catalytically active center for ORR.

Zuo et al. [104] note that the production of highly efficient catalysts for the replacement of platinum in this role in ORR is a very actual scientific and technological task. Authors report a simple method of synthesis of the FeNC catalyst with a 3D hierarchical micro/meso/macroporous network and high surface area by CTF carbonization. The insertion of Fe not only produces the catalytically active Fe–N ... ORR sites and maintains high SSA and abundant pores in the CTF framework during carbonization, but also promotes the formation of mesopores and macropores after acidic leaching. The electrocatalyst FeNC-900 thus demonstrates an excellent ORR activity with a half-wave potential of 0.878 V, 0.40 mV more positive than Pt/C for ORR in basic solution. In acidic solution, the half-wave potential is 0.72 V, which is comparable with Pt/C potential. In particular, FeNC-900 demonstrates significantly higher stability and tolerance to methanol than Pt/C, and this makes it one of the best catalysts among non-precious ones ever reported for ORR.

3.3. Materials for Electrodes

Most often, CTFs are tested as materials for electrodes in supercapacitors [12,19,24,62,63]. Li et al. [24] prepared carbon materials with high SSA and porosity. Preparation obtained at 800 °C and tested as an electrode for the supercapacitor demonstrated the maximal capacitance of 383 F/g at the SSA 3663 m^2/g, with a residual nitrogen content of 8.13%. This material sustained 5000 recharges, retaining 92% specific capacity at a current density of 7 A/g, an energy density of 42.8 W·h/kg, and a power density of 8750 W/kg. Such a high quality of material is provided by the optimal nitrogen content along with other specific properties. High nitrogen content promotes the wettability of the electrode surface with ionic liquid.

CTFs have also been synthesized for usage as anodes in sodium-ionic cells [67,105,112,134]. Polymers possess remarkable strengths and rate capacity (88.8 mA·h/g at current density 5.0 A/g after 1000 cycles) and are promising candidates for highly efficient sodium-ionic cell anodes.

Lithium-sulfur batteries potentially have high energy density—2600 W·h/kg—and therefore materials with high sulfur content are required. Sulfur can be inserted into CTF [98,113] and used for the production of cathode materials in lithium-sulfur batteries. In this material, the triazine cycles promote the dissolution of lithium polysulfides. Such a cathode provides a specific capacity of 1138 mA·h/g.

CIFs are promising as electrodes in lithium-ion batteries [114,115,133]: a specific capacity of 235 mA·h/g was provided after 2500 cycles of recharge at 5 A/g.

CTF was also obtained on the surface of reduced graphene oxide (rGO), and such sandwich CTF/rGO/CTF gave porous carbon doped with nitrogen after pyrolysis; the properties of the obtained carbon were in good accord with the requirements for the electrode materials for fuel cells [30]. The catalytic activity of this material in the catalysis of the oxygen reduction reaction is higher than that of Pt/C.

3.4. Membranes

Energetically efficient and environmentally non-hazardous separation processes are required in various branches of industry. Membrane technology of separation is one of the most promising. Nonetheless, the production of membranes with efficient characteristics of separation is a problem. Ying et al. [103] suggested a way of layer-by-layer CTF application on graphene oxide (GO) in order to produce ultrathin COF membranes for gas separation. Numerous functional groups in GO can improve interactions, arranging 2D CTF-1 on a template; this results in the formation of continuous and dense ultrathin membranes with regulated thickness (100, 200 and 290 nm) via a simple vacuum filtration of liquid dispersion. Different numbers of nanosheets laid in these membranes result in the formation of narrow interlayer channels, which can affect the selective penetration of gas molecules with the regulated selection efficiency. For example, H_2 was separated from CO_2 with

high efficiency and good permeability for H_2 (1.7×10^{-6} mol/m^2·s·Pa) and also with competitive selectivity.

Covalent organic nanoribbons were produced as functional 2D materials for universal usage [116]. Using such frameworks, the authors produced a membrane with a mixed template, which can be useful as an antibacterial cover.

Sasmal et al. [57] note that CTF are especially promising for proton-conductive membranes of fuel cells, because numerous nitrogen atoms have one lone electron pair each, and protons can migrate over them. For this purpose, CTF synthesis is combined with membrane production. Amino-*p*-toluenesulfonic acid (PTSA·H_2O) is used as a filler promoting the maximal porosity of membranes and their high proton conductivity simultaneously.

3.5. Medical Applications

As described, porous solid substances can be used as matrices for the delivery of ibuprofen in vitro [74]. CTFs can be used as a potential transport system for the delivery of drugs and their controlled release [81]. CTFs were exfoliated by intense ultrasonication with subsequent filtration and the obtainment of 2D nanosheets. This product demonstrated an excellent dispersibility in saline solution, retaining its chemical structure and porosity. Doxorubicin (DOX), an anticancer drug, was held on a CTF by hydrophobic interactions, among others, and its release was controlled at pH 4.8 and 7.4. CTF itself did not demonstrate toxicity via cancer cells or normal cells, but the CTF–DOX complex displayed high efficiency against both types of cells in vitro. Visualization of cells in vitro showed that CTF is a potential material for biovisualization. A polymer obtained by Das et al. [56] demonstrated a high anticancer activity against colorectal carcinoma cells. Antibacterial activity of CTF is mentioned by Rajagopal et al. [132].

3.6. Electrotechnical Applications

Only a few electrotechnical applications of CTF are described. CTFs are reported to be good as electrorheological (ER) liquids [77]. ER comprise suspensions of CTF particles easily polarized by the electric field in the insulator liquid phase, and the rheological properties of suspension are reversibly modulated by the external electric field. In the absence of an electric field, CTF particles are occasionally distributed in suspension volume, but at the applied electric field CTF particles are polarized (and thus turn into dipoles) and aggregate with each other into chains due to dipole–dipole interactions. Shear viscosity and shear stress of suspension change significantly, and suspension transforms into an almost solid state. Such suspensions can be potentially used in power drives and analogous devices.

In CTFs, nanolayers often form π–π stacks similar to graphite, or the lone 2D layers collapse into scrolls analogous to graphene. Electrons can migrate along 2D nanolayers and move from layer to layer, thus giving semiconducting and optoelectronic properties to CTFs. A CTF obtained by Kim et al. [92] had a band gap width of 1.91 eV; thereby allowing its usage in optoelectronics as well as in semiconductor devices.

Liu et al. [39] demonstrated the possibility of performing the 2D polymerization of dinitriles at the interphase. The obtained triazine-based 2D polymers had lateral dimensions of several μm and excellent dispersibility in organic solvents; this allowed their conversion in mechanically strong multilayer films with high a SSA via filtration. A crystalline 2D polymer with conjugated bonds in the molecule can act as a semiconducting layer in field-effect transistor devices.

4. Conclusions

CTFs are insoluble in many solvents; their crystallinity is formed during their synthesis by superimposing planar polymer molecules, usually in AA order, and channels causing the porosity of polymers are thus formed. The nature of pores are controlled by dimensions of the linker. Being stochastic, the superposition of layers is not ideal; thus, only the partial overlap of planar molecules is possible. Along with this, polymer molecules differ in lateral size, and relatively small polymer molecules can be located between large molecules.

Besides this, the planarity of molecules can be violated even in the presence of a system of conjugated bonds throughout the molecule. As a result, the crystalline domains of a given polymer are fragmentary and occasionally distributed throughout its volume.

In order to obtain COFs with better crystallinity, modificators are added to the reaction mixture [153,154]. They provide the rapid formation of covalent bonds in the course of synthesis, as well as the rapid breaking and subsequent formation of other covalent bonds. These processes result in the reversibility of COF formation reactions, thermodynamic equilibrium, and the remedying of defects in a crystal. CTF crystallinity is also obtained by very slow mixing the initial solutions [155], or the addition of potassium butylate in the course of synthesis [137]. These examples support our conclusion about the dependence of CTF crystallinity on the methods and conditions of their synthesis.

In the absence of ways to control the thermodynamic equilibrium, it is not easy to recognize one of the abovementioned methods to control a reaction, and thereby analyze the results of the synthesis. Choosing the degree of crystallinity of the obtained polymer as a measure for the input of thermodynamic control, we consider amorphous preparation as the result of kinetic control. We also suppose that the whole product can be a mixture of substances obtained under thermodynamic as well as kinetic control.

CTF crystallinity is affected by solvent (as in any crystallization process), temperature (the higher the temperature, the greater the crystallinity), concentrations of the initial reagents and consequently the rates of the formation of polymers (the slower the rate, the greater crystallinity is), the absence or presence of a catalyst, and so on. However, crystallinity formed in the course of synthesis can be violated during isolation, or the washing and drying of CTF. Therefore, the absence of crystallinity does not allow us to conclude that synthesis was performed under kinetic control. This fact complicates the application of the crystallinity criterion for determination of the type of control.

From the modern viewpoint, reactions under thermodynamic control proceed on the interaction of molecular precursors or their interaction with oligomers already formed. However, being the building blocks, these intermediate polymers can interact with each other, yielding a curious combination of polymeric fragments due to the action of kinetic traps. In this case, polymer molecules structurally differ from each one, being identical in composition. Such a situation is typical of kinetically controlled processes. As polymerization reaction proceeds, the concentration of precursors falls, whereas the concentration of oligomers grows; consequently, thermodynamic control is typical of the beginning of a polymerization reaction, and kinetic control is supposed to dominate in the final stages of a reaction.

Unfortunately, we failed to find studies in which CTFs were synthesized in one and the same solvent, using one and the same catalyst, via one and the same reaction under thermodynamic as well as kinetic control (e.g., at various temperatures).

In summary, we should accept that the relationships between crystallinity/amorphicity, specific surface area, and porosity in CTF polymers are rather complicated. Consequently, it is only possible to formulate the tendencies mentioned above, rather than formulate ways to obtain materials with desired crystallinity, specific surface area, and porosity. As always, the structure and properties of a material in terms of definite composition depend on the conditions of its synthesis.

Funding: This research was funded by RFBR, grant number 20-08-00097.

Conflicts of Interest: The authors declare no conflict of interest.

References

1. Novoselov, K.S.; Geim, A.K.; Morozov, S.V.; Jiang, D.; Katsnelson, M.I.; Grigorieva, I.V.; Dubonos, S.V.; Firsov, A.A. Two-dimensional gas of massless Dirac fermions in graphene. *Nature* **2005**, *438*, 197–200. [CrossRef]
2. Aslanov, L.A.; Dunaev, S.F. Exfoliation of crystals. *Russ. Chem. Rev.* **2018**, *87*, 882–903. [CrossRef]
3. Aslanov, L.A.; Fetisov, G.V.; Paseshnichenko, K.A.; Dunaev, S.F. Liquid phase methods for design and engineering of two-dimensional nanocrystals. *Coord. Chem. Rev.* **2017**, *352*, 220–248. [CrossRef]

4. Kuhn, P.; Antonietti, M.; Thomas, A. Porous, covalent triazine-based frameworks prepared by ionothermal synthesis. *Angew. Chem. Int. Ed.* **2008**, *47*, 3450–3453. [CrossRef] [PubMed]
5. Jia, J.; Chen, Z.; Belmabkhout, Y.; Adil, K.; Bhatt, P.M.; Solovyeva, V.A.; Shekhah, O.; Eddaoudi, M. Carbonization of covalent triazine-based frameworks via ionic liquid induction. *J. Mater. Chem. A* **2018**, *6*, 15564–15568. [CrossRef]
6. Siebels, M.; Schlüsener, C.; Thomas, J.; Xiao, Y.-X.; Yang, X.-Y.; Janiak, C. Rhodium nanoparticles supported on covalent triazine-based frameworks as re-usable catalyst for benzene hydrogenation and hydrogen evolution reaction. *J. Mater. Chem. A* **2019**, *7*, 11934–11943. [CrossRef]
7. Bhunia, A.; Dey, S.; Bous, M.; Zhang, C.; Rybinski, W.; Janiak, C. High adsorptive properties of covalent triazine-based frameworks (CTFs) for surfactants from aqueous solution. *Chem. Commun.* **2015**, *51*, 484–486. [CrossRef]
8. Zheng, H.; Shi, S.; Wang, X.; Zhao, L.; Zhu, G.; Liu, M.; Gao, J.; Xu, J. Covalent triazine frameworks as metal free catalysts for the oxidative coupling of amines to imines. *ChemistrySelect* **2019**, *4*, 5073–5080. [CrossRef]
9. Tuci, G.; Iemhoff, A.; Ba, H.; Luconi, L.; Rossin, A.; Papaefthimiou, V.; Palkovits, R.; Artz, J.; Pham-Huu, C.; Giambastiani, G. Playing with covalent triazine framework tiles for improved CO_2 adsorption properties and catalytic performance. *Beilstein J. Nanotechnol.* **2019**, *10*, 1217–1227. [CrossRef]
10. Schwinghammer, K.; Hug, S.; Mesch, M.B.; Senker, J.; Lotsch, B.V. Phenyl-triazine oligomers for light-driven hydrogen evolution. *Energy Environ. Sci.* **2015**, *8*, 3345–3353. [CrossRef]
11. Zhang, M.; Liu, L.; He, T.; Wu, G.; Chen, P. Synthesis of two-dimensional microporous carbonaceous polymer nanosheets and their application as high-performance CO_2 capture sorbent. *Chem. Asian J.* **2016**, *11*, 1849–1855. [CrossRef] [PubMed]
12. Hao, L.; Ning, J.; Luo, B.; Wang, B.; Zhang, Y.; Tang, Z.; Yang, J.; Thomas, A.; Zhi, L. Structural evolution of 2D microporous covalent triazine-based framework toward the study of high-performance supercapacitors. *J. Am. Chem. Soc.* **2015**, *137*, 219–225. [CrossRef]
13. Xu, R.; Wang, X.-S.; Zhao, H.; Lin, H.; Huang, Y.-B.; Cao, R. Rhenium-modified porous covalent triazine framework for highly efficient photocatalytic carbon dioxide. *Catal. Sci. Technol.* **2018**, *8*, 2224–2230. [CrossRef]
14. Iwase, K.; Yoshioka, T.; Nakanishi, S.; Hashimoto, K.; Kamiya, K. Copper-modified covalent triazine frameworks as non-noble-metal electrocatalysts for oxygen reduction. *Angew. Chem. Int. Ed.* **2015**, *54*, 11068–11072. [CrossRef] [PubMed]
15. Soorholtz, M.; Jones, L.C.; Samuelis, D.; Weidenthaler, C.; White, R.J.; Titirici, M.-M.; Cullen, D.A.; Zimmermann, T.; Antonietti, M.; Maier, J.; et al. Local platinum environments in a solid analogue of the molecular periana catalyst. *ACS Catal.* **2016**, *6*, 2332–2340. [CrossRef]
16. Chang, F.; Guo, J.; Wu, G.; Liu, L.; Zhang, M.; He, T.; Wang, P.; Yu, P.; Chen, P. Covalent triazine-based framework as an efficient catalyst support for ammonia decomposition. *RSC Adv.* **2015**, *5*, 3605–3610. [CrossRef]
17. Artz, J.; Palkovits, R. Base-Free Aqueous-Phase Oxidation of 5-Hydroxymethylfurfural over Ruthenium Catalysts Supported on Covalent Triazine Frameworks. *ChemSusChem* **2015**, *8*, 3832–3838. [CrossRef]
18. Artz, J.; Mallmann, S.; Palkovits, R. Selective aerobic oxidation of HMF to 2,5-diformylfuran on covalent triazine frameworks-supported Ru catalysts. *ChemSusChem* **2015**, *8*, 672–679. [CrossRef]
19. Wang, D.-G.; Wang, H.; Lin, Y.; Yu, G.; Song, M.; Zhong, W.; Kuang, G.-C. Synthesis and morphology evolution of ultrahigh content nitrogen-doped, micropore-dominated carbon materials as high-performance supercapacitors. *ChemSusChem* **2018**, *11*, 3932–3940. [CrossRef]
20. Wang, K.K.; Huang, H.L.; Liu, D.H.; Wang, C.; Li, J.P.; Zhong, C.L. Covalent triazine-based frameworks with ultramicropores and high nitrogen contents for highly selective CO_2 capture. *Environ. Sci. Technol.* **2016**, *50*, 4869–4876. [CrossRef]
21. Wang, Y.; Chen, J.; Wang, G.; Li, Y.; Wen, Z. Perfluorinated covalent triazine framework derived hybrids for the highly selective electroconversion of carbon dioxide into methane. *Angew. Chem. Int. Ed.* **2018**, *57*, 13120–13124. [CrossRef] [PubMed]
22. Gunasekar, G.H.; Jung, K.-D.; Yoon, S. Hydrogenation of CO_2 to formate using a simple, recyclable, and efficient heterogeneous catalyst. *Inorg. Chem.* **2019**, *58*, 3717–3723. [CrossRef] [PubMed]
23. Park, K.; Gunasekar, G.H.; Prakash, N.; Jung, K.-D.; Yoon, S. A highly efficient heterogenized iridium complex for the catalytic hydrogenation of carbon dioxide to formate. *ChemSusChem* **2015**, *8*, 3410–3413. [CrossRef]
24. Li, Y.; Zheng, S.; Liu, X.; Li, P.; Sun, L.; Yang, R.; Wang, S.; Wu, Z.-S.; Bao, X.; Deng, W.-Q. Conductive microporous covalent triazine-based framework for high-performance electrochemical capacitive energy storage. *Angew. Chem. Int. Ed.* **2018**, *57*, 7992–7996. [CrossRef] [PubMed]
25. Lu, Y.; He, J.; Chen, Y.; Wang, H.; Zhao, Y.; Han, Y.; Ding, Y. Effective acetylene/ethylene separation at ambient conditions by a pigment-based covalent-triazine framework. *Macromol. Rapid Commun.* **2018**, *39*, 1700468. [CrossRef]
26. Fu, Y.; Wang, Z.; Fu, X.; Yan, J.; Liu, C.; Pan, C.; Yu, G. Acid/hydrazide-appended covalent triazine frameworks for low-pressure CO_2 capture: Pre-designable or post-synthesis modification. *J. Mater. Chem. A* **2017**, *5*, 21266–21274. [CrossRef]
27. Zhu, X.; Tian, C.; Veith, G.M.; Abney, C.W.; Dehaudt, J.; Dai, S. In situ doping strategy for the preparation of conjugated triazine frameworks displaying efficient CO_2 capture performance. *J. Am. Chem. Soc.* **2016**, *138*, 11497–11500. [CrossRef]
28. Tao, L.M.; Niu, F.; Wang, C.; Liu, J.G.; Wang, T.M.; Wang, Q.H. Benzimidazole functionalized covalent triazine frameworks for CO_2 capture. *J. Mater. Chem. A* **2016**, *4*, 11812–11820. [CrossRef]
29. Yuan, K.Y.; Liu, C.; Han, J.H.; Yu, G.P.; Wang, J.Y.; Duan, H.M.; Wang, Z.G.; Jian, X.G. Phthalazinone structure-based covalent triazine frameworks and their gas adsorption and separation properties. *RSC Adv.* **2016**, *6*, 12009–12020. [CrossRef]

30. Jiao, L.; Hu, Y.; Ju, H.; Wang, C.; Gao, M.-R.; Yang, Q.; Zhu, J.; Yu, S.-H.; Jiang, H.-L. From covalent triazine-based frameworks to N-doped porous carbon/reduced graphene oxide nanosheets: Efficient electrocatalysts for oxygen reduction. *J. Mater. Chem. A* **2017**, *5*, 23170–23178. [CrossRef]
31. Hug, S.; Stegbauer, L.; Oh, H.; Hirscher, M.; Lotsch, B.V. Nitrogen-rich covalent triazine frameworks as high-performance platforms for selective carbon capture and storage. *Chem. Mater.* **2015**, *27*, 8001–8010. [CrossRef]
32. Bavykina, A.V.; Goesten, M.G.; Kapteijn, F.; Makkee, M.; Gascon, J. Efficient production of hydrogen from formic acid using a covalent triazine framework supported molecular catalyst. *ChemSusChem* **2015**, *8*, 809–812. [CrossRef] [PubMed]
33. Krishnaraj, C.; Jena, H.S.; Leus, K.; Freeman, H.M.; Benning, L.G.; Van Der Voort, P. An aliphatic hexene-covalent triazine framework for selective acetylene/methane and ethylene/methane separation. *J. Mater. Chem. A* **2019**, *7*, 13188–13196. [CrossRef]
34. Tao, L.M.; Niu, F.; Liu, J.G.; Wang, T.M.; Wang, Q.H. Troger's base functionalized covalent triazine frameworks for CO_2 capture. *RSC Adv.* **2016**, *6*, 94365–94372. [CrossRef]
35. Gu, C.; Liu, D.; Huang, W.; Liu, J.; Yang, R. Synthesis of covalent triazine-based frameworks with high CO_2 adsorption and selectivity. *Polym. Chem.* **2015**, *6*, 7410–7417. [CrossRef]
36. Zhu, Y.; Chen, X.; Liu, J.; Zhang, J.; Xu, D.; Peng, W.; Li, Y.; Zhang, G.; Zhang, F.; Fan, X. Efficient electrocatalyst for the hydrogen evolution reaction derived from polyoxotungstate/polypyrrole/graphene. *ChemSusChem* **2018**, *11*, 2402–2407. [CrossRef]
37. Bi, J.; Fang, W.; Li, L.; Wang, J.; Liang, S.; He, Y.; Liu, M.; Wu, L. Covalent triazine-based frameworks as visible light photocatalysts for the splitting of water. *Macromol. Rapid Commun.* **2015**, *36*, 1799–1805. [CrossRef]
38. Lan, Z.-A.; Fang, Y.; Zhang, Y.; Wang, X. Photocatalytic Oxygen Evolution from Functional Triazine-Based Polymers with Tunable Band Structures. *Angew. Chem. Int. Ed.* **2018**, *57*, 470–474. [CrossRef]
39. Liu, J.; Zan, W.; Li, K.; Yang, Y.; Bu, F.; Xu, Y. Solution Synthesis of Semiconducting Two-Dimensional Polymer via Trimerization of Carbonitrile. *J. Am. Chem. Soc.* **2017**, *139*, 11666–11669. [CrossRef]
40. Yu, S.; Xu, Y.; Jiang, J.; Ren, S. Room temperature synthesis and substituent effect study of fluorene-based covalent triazine-based frameworks. *Acta Chim. Sin.* **2015**, *73*, 629–633. [CrossRef]
41. Wang, S.F.; Liu, C.B.; Huang, Y.; Hu, Y.C.; Zhang, B. Covalent triazine framework-supported palladium as a ligand-free catalyst for the selective double carbonylation of aryl iodides under ambient pressure of CO. *Chem. Commun.* **2016**, *52*, 2960–2963. [CrossRef] [PubMed]
42. Huang, W.; Byun, J.; Rçrich, I.; Ramanan, C.; Blom, P.W.M.; Lu, H.; Wang, D.; Silva, L.C.; Li, R.; Wang, L.; et al. Asymmetric Covalent Triazine Framework for Enhanced Visible-Light Photoredox Catalysis via Energy Transfer Cascade. *Angew. Chem. Int. Ed.* **2018**, *57*, 8316–8320. [CrossRef] [PubMed]
43. Huang, W.; Wang, Z.J.; Ma, B.C.; Ghasimi, S.; Gehrig, D.; Laquai, F.; Landfester, K.; Zhang, K.A.J. Hollow nanoporous covalent triazine frameworks *via* acid vapor-assisted solid phase synthesis for enhanced visible light photoactivity. *J. Mater. Chem.* **2016**, *4*, 7555–7559. [CrossRef]
44. Wang, X.Y.; Zhang, C.; Zhao, Y.; Ren, S.J.; Jiang, J.X. Synthetic control and multifunctional properties of fluorescent covalent triazine-based frameworks. *Macromol. Rapid Commun.* **2016**, *37*, 323–329. [CrossRef] [PubMed]
45. Puthiaraj, P.; Lee, Y.R.; Zhang, S.Q.; Ahn, W.S. Triazine-based covalent organic polymers: Design, synthesis and applications in heterogeneous catalysis. *J. Mater. Chem. A* **2016**, *4*, 16288–16311. [CrossRef]
46. Karmakar, A.; Kumar, A.; Chaudhari, A.K.; Samanta, P.; Desai, A.V.; Krishna, R.; Ghosh, S.K. Bimodal functionality in a porous covalent triazine framework by rational integration of an electron-rich and -deficient pore surface. *Chem. Eur. J.* **2016**, *22*, 4931–4937. [CrossRef]
47. Kuecken, S.; Schmidt, J.; Zhi, L.; Thomas, A. Conversion of amorphous polymer networks to covalent organic frameworks under ionothermal conditions: A facile synthesis route for covalent triazine frameworks. *J. Mater. Chem. A* **2015**, *3*, 24422–24427. [CrossRef]
48. Kaleeswaran, D.; Antony, R.; Sharma, A.; Malani, A.; Murugavel, R. Catalysis and CO_2 capture by palladium-incorporated covalent organic frameworks. *ChemPlusChem* **2017**, *82*, 1253–1265. [CrossRef]
49. Gomes, R.; Bhanja, P.; Bhaumik, A. A triazine-based covalent organic polymer for efficient CO_2 adsorption. *Chem. Commun.* **2015**, *51*, 10050–10053. [CrossRef]
50. Popp, N.; Homburg, T.; Stock, N.; Senker, J. Porous imine-based networks with protonated imine linkages for carbon dioxide separation from mixtures with nitrogen and methane. *J. Mater. Chem. A* **2015**, *3*, 18492–18504. [CrossRef]
51. Wu, S.; Gu, S.; Zhang, A.; Yu, G.; Wang, Z.; Jian, J.; Pan, C. A rational construction of microporous imide-bridged covalent–organic polytriazines for high-enthalpy small gas absorption. *J. Mater. Chem. A* **2015**, *3*, 878–885. [CrossRef]
52. Halder, A.; Kandambeth, S.; Biswal, B.P.; Kaur, G.; Roy, N.C.; Addicoat, M.; Salunke, J.K.; Banerjee, S.; Vanka, K.; Heine, T.; et al. Decoding the morphological diversity in two dimensional crystalline porous polymers by core planarity modulation. *Angew. Chem. Int. Ed.* **2016**, *55*, 7806–7810. [CrossRef] [PubMed]
53. Gomes, R.; Bhaumik, A. A new triazine functionalized luminescent covalent organic framework for nitroaromatic sensing and CO_2 storage. *RSC Adv.* **2016**, *6*, 28047–28054. [CrossRef]
54. Sadhasivam, V.; Balasaravanan, R.; Chithiraikumar, C.; Siva, A. Incorporating $Pd(OAc)_2$ on imine functionalized microporous covalent organic frameworks: A stable and efficient heterogeneous catalyst for Suzuki-Miyaura coupling in aqueous medium. *ChemistrySelect* **2017**, *2*, 1063–1070. [CrossRef]
55. Fan, X.; Tian, R.; Liu, S.; Qiao, S.; Luo, Q.; Yan, T.; Fu, S.; Zhang, X.; Xu, J.; Liu, J. Covalently assembled polymer nanocapsules: A novel scaffold for light-harvesting. *Polym. Chem.* **2018**, *9*, 1160–1163. [CrossRef]

56. Das, S.K.; Mishra, S.; Manna, K.; Kayal, U.; Mahapatra, S.; Saha, K.D.; Dalapati, S.; Das, G.P.; Mostafa, A.A.; Bhaumik, A. A new triazine based π-conjugated mesoporous 2D covalent organic framework: Its in vitro anticancer activities. *Chem. Commun.* **2018**, *54*, 11475–11478.
57. Sasmal, H.S.; Aiyappa, H.B.; Bhange, S.N.; Karak, S.; Halder, A.; Kurungot, S.; Banerjee, R. Superprotonic conductivity in flexible porous covalent organic framework membranes. *Angew. Chem. Int. Ed.* **2018**, *57*, 10894–10898. [CrossRef]
58. Guo, L.; Niu, Y.; Xu, H.; Li, Q.; Razzaque, S.; Huang, Q.; Jin, S.; Tan, B. Engineering heteroatoms with atomic precision in donor–acceptor covalent triazine frameworks to boost photocatalytic hydrogen production. *J. Mater. Chem. A* **2018**, *6*, 19775–19781. [CrossRef]
59. Xu, N.; Wang, R.-L.; Li, D.-P.; Meng, X.; Mu, J.-L.; Zhou, Z.-Y.; Su, Z.-M. A new triazine-based covalent organic polymer for efficient photodegradation of both acidic and basic dyes under visible light. *Dalton Trans.* **2018**, *47*, 4191–4197. [CrossRef]
60. Zhang, M.; Zheng, R.; Ma, Y.; Chen, R.; Sun, X. N-rich covalent organic frameworks with different pore size for high-pressure CO_2 adsorption. *Microporous Mesoporous Mater.* **2019**, *285*, 70–79. [CrossRef]
61. Bhadra, M.; Kandambeth, S.; Sahoo, M.K.; Addicoat, M.; Balaraman, E.; Banerjee, R. Triazine Functionalized Porous Covalent Organic Framework for Photo-organocatalytic E–Z Isomerization of Olefins. *J. Am. Chem. Soc.* **2019**, *141*, 6152–6156. [CrossRef] [PubMed]
62. Li, Y.; Liu, L.; Wu, Y.; Wu, T.; Wu, H.; Cai, Q.; Xu, Y.; Zeng, B.; Yuan, C.; Dai, L. Facile synthesis of nitrogen-doped carbon materials with hierarchical porous structures for high-performance supercapacitors in both acidic and alkaline electrolytes. *J. Mater. Chem. A* **2019**, *7*, 13154–13163. [CrossRef]
63. El-Mahdy, A.F.M.; Hung, Y.-H.; Mansoure, T.H.; Yu, H.-H.; Chen, T.; Kuo, S.-W. A hollow microtubular triazine- and benzobisoxazole-based covalent organic framework presenting sponge-like shells that functions as a high-performance supercapacitor. *Chem. Asian J.* **2019**, *14*, 1429–1435. [CrossRef] [PubMed]
64. Yu, S.-Y.; Mahmood, J.; Noh, H.-J.; Seo, J.-M.; Jung, S.-M.; Shin, S.-H.; Im, Y.-K.; Jeon, I.-Y.; Baek, J.-B. Direct synthesis of a covalent triazine-based framework from aromatic amides. *Angew. Chem. Int. Ed.* **2018**, *57*, 8438–8442. [CrossRef] [PubMed]
65. Chen, X.; Addicoat, M.; Jin, E.; Xu, H.; Hayashi, T.; Xu, F.; Huang, N.; Irle, S.; Jiang, D. Designed synthesis of double-stage two-dimensional covalent organic frameworks. *Sci. Rep.* **2015**, *5*, 14650. [CrossRef] [PubMed]
66. Liao, Y.; Weber, J.; Faul, C.F.J. Fluorescent microporous polyimides based on perylene and triazine for highly CO_2-selective carbon materials. *Macromolecules* **2015**, *48*, 2064–2073. [CrossRef]
67. Li, Z.T.; Zhou, J.Y.; Xu, R.F.; Liu, S.P.; Wang, Y.K.; Li, P.; Wu, W.T.; Wu, M.B. Synthesis of three dimensional extended conjugated polyimide and application as sodium-ion battery anode. *Chem. Eng. J.* **2016**, *287*, 516–522. [CrossRef]
68. Chen, X.; Addicoat, M.; Jin, E.; Zhai, L.; Xu, H.; Huang, N.; Guo, Z.; Liu, L.; Irle, S.; Jiang, D. Locking covalent organic frameworks with hydrogen bonds: General and remarkable effects on crystalline structure, physical properties, and photochemical activity. *J. Am. Chem. Soc.* **2015**, *137*, 3241–3247. [CrossRef]
69. Puthiaraj, P.; Yu, K.; Shim, S.E.; Ahn, W.-S. Pd(II)-immobilized on a nanoporous triazine-based covalent imine framework for facile cyanation of haloarenes with $K_4Fe(CN)_6$. *Mol. Catal.* **2019**, *473*, 110395. [CrossRef]
70. Lin, S.; Hou, Y.; Deng, X.; Wang, H.; Sun, S.; Zhang, X. A triazine-based covalent organic framework/palladium hybrid for one-pot silicon-based cross-coupling of silanes and aryl iodides. *RSC Adv.* **2015**, *5*, 41017–41024. [CrossRef]
71. Xu, L.Q.; Ding, S.Y.; Liu, J.M.; Sun, J.L.; Wang, W.; Zheng, Q.Y. Highly crystalline covalent organic frameworks from flexible building blocks. *Chem. Commun.* **2016**, *52*, 4706–4709. [CrossRef] [PubMed]
72. Das, S.K.; Wang, X.; Ostwal, M.M.; Lai, Z. A highly stable microporous covalent imine network adsorbent for natural gas upgrading and flue gas CO_2 capture. *Sep. Purif. Technol.* **2016**, *170*, 68–77. [CrossRef]
73. Puthiaraj, P.; Ahn, W.-S.J. Facile synthesis of microporous carbonaceous materials derived from a covalent triazine polymer for CO_2 capture. *Energy Chem.* **2017**, *26*, 965–971. [CrossRef]
74. Luo, Y.; Liu, J.; Liu, Y.; Lyu, Y.J. Porphyrin-based covalent triazine frameworks: Porosity, adsorption performance, and drug delivery. *Polym. Sci. Part A Polym. Chem.* **2017**, *55*, 2594–2600. [CrossRef]
75. Puthiaraj, P.; Ahn, W.S. Synthesis of copper nanoparticles supported on a microporous covalent triazine polymer: An efficient and reusable catalyst for *O*-arylation reaction. *Catal. Sci. Technol.* **2016**, *6*, 1701–1709. [CrossRef]
76. Yang, W.; Wu, X.; Liu, T.; Wang, T.; Hou, X. A triazine-based conjugated microporous polymer composite for magnetic solid phase extraction of 5-nitroimidazoles coupled with UPLC-MS/MS for quantification. *Analyst* **2018**, *143*, 5744–5753. [CrossRef]
77. Dong, Y.Z.; Kwon, S.H.; Choi, H.J.; Puthiaraj, P.; Ahn, W.-S. Electrorheological response of microporous covalent triazine-based polymeric particles. *Colloid Polym. Sci.* **2018**, *296*, 907–915. [CrossRef]
78. Ravi, S.; Puthiaraj, P.; Park, D.-W.; Ahn, W.-S. Cycloaddition of CO_2 and epoxides over a porous covalent triazine-based polymer incorporated with Fe_3O_4. *New J. Chem.* **2018**, *42*, 12429–12436. [CrossRef]
79. Zhao, W.; Zuo, H.; Guo, Y.; Liu, K.; Wang, S.; He, L.; Jiang, X.; Xiang, G.; Zhang, S. Porous covalent triazine-terphenyl polymer as hydrophilic-lipophilic balanced sorbent for solid phase extraction of tetracyclines in animal derived foods. *Talanta* **2019**, *201*, 426–432. [CrossRef]
80. Geng, T.; Zhang, W.; Zhu, Z.; Kai, X. Triazine-based conjugated microporous polymers constructing triphenylamine and its derivatives with nitrogen as core for iodine adsorption and fluorescence sensing I_2. *Microporous Mesoporous Mater.* **2019**, *273*, 163–170. [CrossRef]
81. Rengaraj, A.; Puthiaraj, P.; Haldorai, Y.; Heo, N.S.; Hwang, S.K.; Han, Y.K.; Kwon, S.; Ahn, W.S.; Huh, Y.S. Porous covalent triazine polymer as a potential nanocargo for cancer therapy and imaging. *ACS Appl. Mater. Interfaces* **2016**, *8*, 8947–8955. [CrossRef]

82. Shao, L.; Wang, S.; Liu, M.; Huang, J.; Liu, Y.-N. Triazine-based hyper-cross-linked polymers derived porous carbons for CO_2 capture. *Chem. Eng. J.* **2018**, *339*, 509–518. [CrossRef]
83. Fu, X.; Zhang, Y.; Gu, S.; Zhu, Y.; Yu, G.; Pan, C.; Wang, Z.; Hu, Y. Metal microporous aromatic polymers with improved performance for small gas storage. *Chem. Eur. J.* **2015**, *21*, 13357–13363. [CrossRef] [PubMed]
84. Chaudhary, M.; Muhammad, R.; Ramachandran, C.N.; Mohanty, P. Nitrogen amelioration-driven carbon dioxide capture by nanoporous polytriazine. *Langmuir* **2019**, *35*, 4893–4901. [CrossRef]
85. Lee, S.-P.; Mellon, N.; Shariff, A.M.; Leveque, J.-M. Geometry variation in porous covalent triazine polymer (CTP) for CO_2 adsorption. *New J. Chem.* **2018**, *42*, 15488–15496. [CrossRef]
86. Xiong, S.; Tao, J.; Wang, Y.; Tang, J.; Liu, C.; Liu, Q.; Wang, Y.; Yu, G.; Pan, C. Uniform poly(phosphazene–triazine) porous microspheres for highly efficient iodine removal. *Chem. Commun.* **2018**, *54*, 8450–8453. [CrossRef] [PubMed]
87. Yang, C.; Huang, W.; Silva, L.C.; Zhang, K.A.I.; Wang, X. Functional conjugated polymers for CO_2 reduction using visible light. *Chem. Eur. J.* **2018**, *24*, 17454–17458. [CrossRef]
88. Wang, J.; Harrison, M. Removal of organic micro-pollutants from water by β-cyclodextrin triazine polymers. *J. Incl. Phenom. Macrocycl. Chem.* **2018**, *92*, 347–356. [CrossRef]
89. Zhao, Y.; Liu, H.; Wu, C.; Zhang, Z.; Pan, Q.; Hu, F.; Wang, R.; Li, P.; Huang, X.; Li, Z. Fully conjugated two-dimensional sp^2-carbon covalent organic frameworks as artificial photosystem I with high efficiency. *Angew. Chem. Int. Ed.* **2019**, *58*, 5376–5381. [CrossRef]
90. Song, J.-R.; Duan, W.-G.; Li, D.-P. Synthesis of nitrogen-rich polymers by click polymerization reaction and gas sorption property. *Molecules* **2018**, *23*, 1732. [CrossRef]
91. Yao, L.; Rahmanudin, A.; Jeanbourquin, X.A.; Yu, X.; Johnson, M.; Guijarro, N.; Sekar, A.; Sivula, K. Catalyst-free, fast, and tunable synthesis for robust covalent polymer network semiconducting thin films. *Adv. Funct. Mater.* **2018**, *28*, 1706303. [CrossRef]
92. Kim, M.-S.; Phang, C.S.; Jeong, Y.K.; Park, J.K. A facile synthetic route for the morphology-controlled formation of triazine-based covalent organic nanosheets (CONs). *Polym. Chem.* **2017**, *8*, 5655–5659. [CrossRef]
93. Li, Z.; Han, Y.; Guo, Y.; Xu, S.; Chen, F.; Ye, L.; Luo, Z.; Liu, X.; Zhou, H.; Zhao, T. Evolution of the formation of a covalent triazine-based framework catalyzed by *p*-toluenesulfonic acid monohydrate. *RSC Adv.* **2017**, *7*, 45818–45823. [CrossRef]
94. Rehman, A.; Park, S.-J. Preparation and characterization of polyamides and nitrogen-doped carbons for enhanced CO_2 capture. *Bull. Korean Chem. Soc.* **2017**, *38*, 1285–1292. [CrossRef]
95. Yadav, R.K.; Kumar, A.; Park, N.J.; Kong, K.J.; Baeg, J.O. A highly efficient covalent organic framework film photocatalyst for selective solar fuel production from CO_2. *J. Mater. Chem. A* **2016**, *4*, 9413–9418. [CrossRef]
96. Nandi, S.; Werner-Zwanziger, U.; Vaidhyanathan, R. A triazine–resorcinol based porous polymer with polar pores and exceptional surface hydrophobicity showing CO_2 uptake under humid conditions. *J. Mater. Chem. A* **2015**, *3*, 21116–21122. [CrossRef]
97. Talapaneni, S.N.; Hwang, T.H.; Je, S.H.; Buyukcakir, O.; Choi, J.W.; Coskun, A. Elemental-sulfur-mediated facile synthesis of a covalent triazine framework for high-performance lithium–sulfur batteries. *Angew. Chem. Int. Ed.* **2016**, *55*, 3106–3111. [CrossRef]
98. Je, S.H.; Kim, H.J.; Kim, J.; Choi, J.W.; Coskun, A. Perfluoroaryl-elemental sulfur S_NAr chemistry in covalent triazine frameworks with high sulfur contents for lithium–sulfur batteries. *Adv. Funct. Mater.* **2017**, *27*, 1703947. [CrossRef]
99. Liu, J.; Hu, Y.; Cao, J. Covalent triazine-based frameworks as efficient metal-free electrocatalysts for oxygen reduction reaction in alkaline media. *Catal. Commun.* **2015**, *66*, 91–94. [CrossRef]
100. Wang, B.; Lee, L.S.; Wei, C.; Fu, H.; Zheng, S.; Xu, Z.; Zhu, D. Covalent triazine-based framework: A promising adsorbent for removal of perfluoroalkyl acids from aqueous solution. *Environ. Pollut.* **2016**, *216*, 884–892. [CrossRef]
101. He, T.; Liu, L.; Wu, G.; Chen, P. Covalent triazine framework-supported palladium nanoparticles for catalytic hydrogenation of N-heterocycles. *J. Mater. Chem. A* **2015**, *3*, 16235–16241. [CrossRef]
102. Zhong, C.; He, M.; Liao, H.; Chen, B.; Wang, C.; Hu, B. Polydimethylsiloxane/covalent triazine frameworks coated stir bar sorptive extraction coupled with high performance liquid chromatography-ultraviolet detection for the determination of phenols in environmental water samples. *J. Chromatogr. A* **2016**, *1441*, 8–15. [CrossRef] [PubMed]
103. Ying, Y.P.; Liu, D.H.; Ma, J.; Tong, M.M.; Zhang, W.X.; Huang, H.L.; Zhong, Q.Y.; Zhong, C.L. A GO-assisted method for the preparation of ultrathin covalent organic framework membranes for gas separation. *J. Mater. Chem. A* **2016**, *4*, 13444–13449. [CrossRef]
104. Zuo, Q.; Zhao, P.P.; Luo, W.; Cheng, G.Z. Hierarchically porous Fe–N–C derived from covalent-organic materials as a highly efficient electrocatalyst for oxygen reduction. *Nanoscale* **2016**, *8*, 14271–14277. [CrossRef]
105. Liu, J.; Lyu, P.; Zhang, Y.; Nachtigall, P.; Xu, Y. New layered triazine framework/exfoliated 2D polymer with superior sodium-storage properties. *Adv. Mater.* **2018**, *30*, 1705401. [CrossRef]
106. Li, L.Y.; Fang, W.; Zhang, P.; Bi, J.H.; He, Y.H.; Wang, J.Y.; Su, W.Y. Sulfur-doped covalent triazine-based frameworks for enhanced photocatalytic hydrogen evolution from water under visible light. *J. Mater. Chem. A* **2016**, *4*, 12402–12406. [CrossRef]
107. Puthiaraj, P.; Cho, S.-M.; Lee, Y.-R.; Ahn, W.-S. Microporous covalent triazine polymers: Efficient Friedel–Crafts synthesis and adsorption/storage of CO_2 and CH_4. *J. Mater. Chem. A* **2015**, *3*, 6792–6797. [CrossRef]
108. He, X.; Zhang, S.-Y.; Tang, X.; Xiong, S.; Ai, C.; Chen, D.; Tang, J.; Pan, C.; Yu, G. Exploration of 1D channels in stable and high-surface-area covalent triazine polymers for effective iodine removal. *Chem. Eng. J.* **2019**, *371*, 314–318. [CrossRef]
109. Mane, S.; Gao, Z.-Y.; Li, Y.-X.; Xue, D.-M.; Liu, X.-Q.; Sun, L.-B. Fabrication of microporous polymers for selective CO_2 capture: The significant role of crosslinking and crosslinker length. *J. Mater. Chem. A* **2017**, *5*, 23310–23318. [CrossRef]

110. Jiang, X.; Wang, P.; Zhao, J. 2D covalent triazine framework: A new class of organic photocatalyst for water splitting. *J. Mater. Chem. A* **2015**, *3*, 7750–7758. [CrossRef]
111. Guiglion, P.; Butchosa, C.; Zwijnenburg, M.A. Polymer Photocatalysts for Water Splitting: Insights from Computational Modeling. *Macromol. Chem. Phys.* **2016**, *217*, 344–353. [CrossRef]
112. Wang, K.; Yang, L.-M.; Wang, X.; Guo, L.; Cheng, G.; Zhang, C.; Jin, S.; Tan, B.; Cooper, A. Covalent Triazine Frameworks via a Low-Temperature Polycondensation ApproachAngew. *Chem. Int. Ed.* **2017**, *56*, 14149–14153. [CrossRef] [PubMed]
113. Shan, J.Q.; Liu, Y.X.; Su, Y.Z.; Liu, P.; Zhuang, X.D.; Wu, D.Q.; Zhang, F.; Feng, X.L. Graphene-directed two-dimensional porous carbon frameworks for high-performance lithium–sulfur battery cathodes. *J. Mater. Chem. A* **2016**, *4*, 314–320. [CrossRef]
114. Yuan, R.; Kang, W.; Zhang, C. Rational design of porous covalent triazine-based framework composites as advanced organic lithium-ion battery cathodes. *Materials* **2018**, *11*, 937. [CrossRef]
115. Zhu, J.; Zhuang, X.; Yang, J.; Feng, X.; Hirano, S.-I. Graphene-coupled nitrogen-enriched porous carbon nanosheets for energy storage. *J. Mater. Chem. A* **2017**, *5*, 16732–16739. [CrossRef]
116. Mitra, S.; Kandambeth, S.; Biswal, B.P.; Khayum, M.A.; Choudhury, C.K.; Mehta, M.; Kaur, G.; Banerjee, S.; Prabhune, A.; Verma, S.; et al. Self-Exfoliated Guanidinium-Based Ionic Covalent Organic Nanosheets (iCONs). *J. Am. Chem. Soc.* **2016**, *138*, 2823–2828. [CrossRef]
117. Wang, H.; Jiang, D.H.; Huang, D.L.; Zeng, G.M.; Xu, P.; Lai, C.; Chen, M.; Cheng, M.; Zhang, C.; Wang, Z.W. Covalent triazine frameworks for carbon dioxide capture. *J. Mater. Chem. A* **2019**, *7*, 22848–22870. [CrossRef]
118. Tahir, N.; Krishnaraj, C.; Leus, K.; Van der Voort, P. Development of covalent triazine frameworks as heterogeneous catalytic supports. *Polymers* **2019**, *11*, 1326. [CrossRef]
119. Liu, M.Y.; Guo, L.P.; Jin, S.B.; Tan, B.E. Covalent triazine frameworks: Synthesis and applications. *J. Mater. Chem. A* **2019**, *7*, 5153–5172. [CrossRef]
120. Zhang, Y.; Jin, S.B. Recent advancements in the synthesis of cvalent triazine frameworks for energy and environmental applications. *Polymers* **2019**, *11*, 31. [CrossRef]
121. Artz, J. Covalent triazine-based frameworks—Tailor-made catalysts and catalyst supports for molecular and nanoparticulate species. *ChemCatChem* **2018**, *10*, 1753–1771. [CrossRef]
122. Wang, J.; Zhang, K.; Wang, E. Kinetic paths, time scale, and underlying landscapes: A path integral framework to study global natures of nonequilibrium systems and networks. *J. Chem. Phys.* **2010**, *133*, 125103. [CrossRef]
123. Cheetham, A.K.; Kieslich, G.; Yeung, H.H.-M. Thermodynamic and kinetic effects in the crystallization of metal–organic frameworks. *Acc. Chem. Res.* **2018**, *51*, 659–667. [CrossRef]
124. Ji, Q.; Lirag, R.C.; Miljanic, O.S. Kinetically controlled phenomena in dynamic combinatorial libraries. *Chem. Soc. Rev.* **2014**, *43*, 1873–1884. [CrossRef]
125. Janica, I.; Patroniak, V.; Samor, P.; Ciesielski, A. Imine-based architectures at surfaces and interfaces: From self-assembly to dynamic covalent chemistry in 2D. *Chem. Asian J.* **2018**, *13*, 465–481. [CrossRef]
126. Yuan, K.; Hu, T.; Xu, Y.; Graf, R.; Shi, L.; Forster, M.; Pichler, T.; Riedl, T.; Chen, Y.; Scherf, U. Nitrogen-doped porous carbon/graphene nanosheets derived from two-dimensional conjugated microporous polymer sandwiches with promising capacitive performance. *Mater. Chem. Front.* **2017**, *1*, 278–285. [CrossRef]
127. Ohtsu, H.; Kawano, M. Kinetic assembly of coordination networks. *Chem. Commun.* **2017**, *53*, 8818–8829. [CrossRef]
128. Cheetham, A.K.; Rao, C.N.; Feller, R.F. Structural diversity and chemical trends in hybrid inorganic–organic framework materials. *Chem. Commun.* **2006**, *46*, 4780–4795. [CrossRef]
129. Kawano, M.; Haneda, T.; Hashizume, D.; Izumi, F.; Fujita, M. A selective instant synthesis of a coordination network and its ab initio powder structure determination. *Angew. Chem. Int. Ed.* **2008**, *47*, 1269–1271. [CrossRef]
130. Mullin, J.W. *Crystallization*, 4th ed.; Butterworth-Heinemann: Oxford, UK, 2001; 600p.
131. Rieger, J.; Frechen, T.; Cox, G.; Heckmann, W.; Schmidt, C.; Thieme, J. Precursor structures in the crystallization/precipitation processes of $CaCO_3$ and control of particle formation by polyelectrolytes. *Farad. Discuss.* **2007**, *136*, 265–277. [CrossRef]
132. Rajagopal, V.; Narayanan, N.J.; Kathiresan, M.; Pattanayak, D.K.; Suryanarayanan, V. Triazine interlinked covalent organic polymer as an efficient anti-bacterial agent. *Mater. Today Chem.* **2021**, *19*, 100408. [CrossRef]
133. Chen, S.; Wang, S.K.; Xue, X.; Zhao, J.S.; Du, H.M. The synthesis of a covalent organic framework from thiophene armed triazine and EDOT and its application as anode material in lithium-ion battery. *Polymers* **2021**, *13*, 3300. [CrossRef] [PubMed]
134. Yang, N.; Gu, Y.; Shan, Y.; Tian, C.; Yang, L.; Jiang, H.; Liu, H.; Zhu, X.; Dai, S. Dual rate-modulation approach for the preparation of crystalline covalent triazine frameworks displaying efficient sodium storage. *ACS Macro Lett.* **2022**, *11*, 60–65. [CrossRef]
135. Guo, L.P.; Wang, X.P.; Zhan, Z.; Zhao, Y.L.; Chen, L.J.; Liu, T.; Tan, B.E.; Jin, S.B. Crystallization of covalent triazine frameworks via a heterogeneous nucleation approach for efficient photocatalytic applications. *Chem. Mater.* **2021**, *33*, 1994–2003. [CrossRef]
136. Yang, Z.L.; Gu, Y.Y.; Yuan, B.L.; Tian, Y.M.; Shang, J.; Tsang, D.C.W.; Liu, M.X.; Gan, L.H.; Mao, S.; Li, L.C. Thio-groups decorated covalent triazine frameworks for selective mercury removal. *J. Hazard. Mater.* **2021**, *403*, 123702. [CrossRef]
137. Zhang, S.Q.; Cheng, G.; Guo, L.P.; Wang, N.; Tan, B.E.; Jin, S.B. Strong-base-assisted synthesis of a crystalline covalent triazine framework with high hydrophilicity via benzylamine monomer for photocatalytic water splitting. *Angew. Chem. Int. Ed.* **2020**, *59*, 6007–6014. [CrossRef]

138. Afshari, M.; Dinari, M. Synthesis of new imine-linked covalent organic framework as high efficient absorbent and monitoring the removal of direct fast scarlet 4BS textile dye based on mobile phone colorimetric platform. *J. Hazard. Mater.* **2020**, *385*, 121514. [CrossRef]
139. Mokhtari, N.; Khataei, M.M.; Dinari, M.; Monjezi, B.H.; Yamini, Y. Imine-based covalent triazine framework: Synthesis, characterization, and evaluation its adsorption. *Mater. Lett.* **2020**, *263*, 127221. [CrossRef]
140. Wessely, I.D.; Schade, A.M.; Dey, S.; Bhunia, A.; Nuhnen, A.; Janiak, C.; Brase, S. Covalent triazine frameworks based on the first pseudo-octahedral hexanitrile monomer via nitrile trimerization: Synthesis, porosity, and CO_2 gas sorption properties. *Materials* **2021**, *14*, 3214. [CrossRef]
141. Xu, T.T.; Li, Y.; Zhao, Z.Q.; Xing, G.L.; Chen, L. N,N′-Bicarbazol-based covalent triazine frameworks as high-performance heterogeneous photocatalysts. *Macromolecules* **2019**, *52*, 9786–9791. [CrossRef]
142. Gong, R.; Yang, L.; Qiu, S.; Chen, W.T.; Wang, Q.; Xie, J.; Waterhouse, G.I.N.; Xu, J. A Nitrogen-rich covalent triazine framework as a photocatalyst for hydrogen production. *Adv. Polym. Technol.* **2020**, *2020*, 7819049. [CrossRef]
143. Guan, L.J.; Cheng, G.; Tan, B.E.; Jin, S.B. Covalent triazine frameworks constructed via benzyl halide monomers showing high photocatalytic activity in biomass reforming. *Chem. Commun.* **2021**, *57*, 5147–5150. [CrossRef]
144. Wang, G.H.; Zhou, T.; Lei, Y.Q. Exploration of a novel triazine-based covalent organic framework for solid-phase extraction of antibiotics. *RSC Adv.* **2021**, *10*, 11557–11564. [CrossRef]
145. Xu, Y.; Yu, H.T.; Shi, B.Y.; Gao, S.G.; Zhang, L.; Li, X.H.; Liao, X.J.; Huang, K. Room-temperature synthesis of hollow carbazole based covalent triazine polymers with multiactive sites for efficient iodine capture-catalysis cascade application. *ASC Appl. Polym. Mater.* **2020**, *2*, 3704–3713. [CrossRef]
146. EL-Mahdy, A.F.M.; Liu, T.E.; Kuo, S.W. Direct synthesis of nitrogen-doped mesoporous carbons from triazine-functionalized resol for CO_2 uptake and highly efficient removal of dyes. *J. Hazard. Mater.* **2020**, *391*, 122163. [CrossRef]
147. Cui, Z.W.; Hu, Y.; Zhang, Y.K.; Han, Q.T.; Wang, Y.; Zhou, Y.; Zou, Z.G. A new triazine-based conjugated polymer from simple monomers with stable photocatalytic hydrogen evolution under visible light. *Polymer* **2020**, *211*, 123079. [CrossRef]
148. Wang, R.; Xi, S.C.; Wang, D.Y.; Dou, M.; Dong, B. Defluorinated porous carbon nanomaterials for CO_2 capture. *ACS Appl. Nano Mater.* **2021**, *4*, 10148–10154. [CrossRef]
149. Luo, Y.-H.; Ma, S.-H.; Dong, H.; Zou, Y.-C.; Xu, K.-X.; Su, S.; Jin, X.-W.; Zhang, L.; Fang, W.-X. Two-dimensional nanosheets of metal-organic frameworks with tailorable morphologies. *Mater. Today Chem.* **2021**, *22*, 100517. [CrossRef]
150. Luo, Y.-H.; Zhang, L.; Fang, W.-X.; Ma, S.-H.; Dong, H.; Su, S.; Zheng, Z.-Y.; Lia, D.-N.; Zhaib, L.-H. 2D hydrogen-bonded organic frameworks: In-site generation and subsequent exfoliation. *Chem. Commun.* **2021**, *57*, 5901–5904. [CrossRef]
151. Luo, Y.-H.; Wang, C.; Ma, S.-H.; Jin, X.-W.; Zou, Y.-C.; Xu, K.-X.; Fang, W.-X.; Zhang, L.; Dong, H. Humidity reduction by using hetero-layered metal–organic framework nanosheet composites as hygroscopic materials. *Environ. Sci. Nano* **2021**, *8*, 3665–3672. [CrossRef]
152. Krishnaraj, C.; Jena, H.S.; Leus, K.; Van Der Voort, P. Covalent triazine frameworks—A sustainable perspective. *Green Chem.* **2020**, *22*, 1038–1071. [CrossRef]
153. Calik, M.; Sick, T.; Dogru, M.; Doblinger, M.; Datz, S.; Budde, H.; Hartschuh, A.; Auras, F.; Bein, T. From highly crystalline to outer surface-functionalized covalent organic frameworks—A modulation approach. *J. Am. Chem. Soc.* **2016**, *138*, 1234–1239. [CrossRef] [PubMed]
154. Zhu, D.; Alemany, L.B.; Guob, W.; Verduzco, R. Enhancement of crystallinity of imine-linked covalent organic frameworks via aldehyde modulators. *Polym. Chem.* **2020**, *11*, 4464–4468. [CrossRef]
155. Liu, M.; Jiang, K.; Ding, X.; Wang, S.; Zhang, C.; Liu, J.; Zhan, Z.; Cheng, G.; Li, B.; Chen, H.; et al. Controlling monomer feeding rate to achieve highly crystalline covalent triazine frameworks. *Adv. Mater.* **2019**, *31*, 1807865. [CrossRef]